

## Field-aligned coordinates for nonlinear simulations of tokamak turbulence

M. A. Beer, S. C. Cowley, and G. W. Hammett

Citation: *Physics of Plasmas* **2**, 2687 (1995); doi: 10.1063/1.871232

View online: <http://dx.doi.org/10.1063/1.871232>

View Table of Contents: <http://scitation.aip.org/content/aip/journal/pop/2/7?ver=pdfcov>

Published by the AIP Publishing

---

### Articles you may be interested in

[Action at distance and Bohm scaling of turbulence in tokamaks](#)

*Phys. Plasmas* **3**, 1898 (1996); 10.1063/1.871985

[Spatial coherence of a sound field in a refractive shadow: Comparison of simulation and experiment](#)

*J. Acoust. Soc. Am.* **98**, 2289 (1995); 10.1121/1.413343

[Broadband density fluctuation measurements using a heavy ion beam probe on the Texas Experimental Tokamak](#)

*Phys. Plasmas* **2**, 3360 (1995); 10.1063/1.871170

[Effects of edge plasma turbulence on radial correlation length measurements with BES](#)

*Rev. Sci. Instrum.* **63**, 4931 (1992); 10.1063/1.1143553

[Neutral beam emission spectroscopy diagnostic for measurement of density fluctuations on the TFTR tokamak](#)

*Rev. Sci. Instrum.* **61**, 3496 (1990); 10.1063/1.1141557

---



*High Peak Power Femtosecond Lasers*

- Peak Powers to 1PW
- Contrast < 1:10<sup>12</sup>
- Advanced Control System (GUI)

Amplitude Laser Group  
Continuum | Amplitude Technologies | Amplitude Systèmes  
140 Baytech Drive, San Jose, CA 95134, USA

**Continuum**<sup>®</sup>  
[www.continuumlasers.com](http://www.continuumlasers.com)

# Field-aligned coordinates for nonlinear simulations of tokamak turbulence

M. A. Beer, S. C. Cowley,<sup>a)</sup> and G. W. Hammett  
Princeton University Plasma Physics Laboratory, Princeton, New Jersey 08543

(Received 17 October 1994; accepted 15 March 1995)

Turbulence in tokamaks is characterized by long parallel wavelengths and short perpendicular wavelengths. A coordinate system for nonlinear fluid, gyrokinetic "Vlasov," or particle simulations is presented that exploits the elongated nature of the turbulence by resolving the minimum necessary simulation volume: a long thin twisting flux tube. It is very similar to the ballooning representation, although periodicity constraints can be incorporated in a manner that allows  $\mathbf{E} \times \mathbf{B}$  nonlinearities to be evaluated efficiently with fast Fourier transforms (FFT's). If the parallel correlation length is very long, however, enforcing periodicity can introduce artificial correlations, so periodicity should not necessarily be enforced in the poloidal angle at  $\theta = \pm \pi$ . This method is applied to high resolution three-dimensional simulations of toroidal ion temperature gradient (ITG) driven turbulence, which predict fluctuation spectra and ion heat transport similar to experimental measurements. © 1995 American Institute of Physics.

## I. INTRODUCTION

The turbulence that evolves from fine-scale instabilities (e.g.,  $\eta_i$ , trapped electron, or resistive ballooning modes) is thought to be responsible for the anomalously large particle, momentum, and heat transport levels in tokamaks. It is therefore of great interest to simulate numerically the nonlinear evolution of these instabilities to determine the resulting fluctuation and transport levels. These instabilities are characterized by long wavelengths parallel to the magnetic field and short perpendicular wavelengths, on the order of the ion gyroradius,  $\rho_i$ . This is, of course, a consequence of the rapid communication along field lines (at the sound speed for electrostatic instabilities) and slow communication across the field lines (typically velocities across the field do not exceed the diamagnetic speed). In addition, fluctuation measurements<sup>1,2</sup> in tokamaks indicate a relatively short perpendicular correlation length ( $\sim 10\rho_i$ ), but a long parallel correlation length.<sup>3</sup> Simulation of a full tokamak with adequate resolution of these fine perpendicular scales is somewhat beyond the presently available computational resources, since  $\rho_i/a \sim 10^{-3}$  for present day large tokamaks, where  $a$  is the minor radius. (The latest full torus gyrokinetic particle simulations can now be run down to  $\rho_i/a = \frac{1}{128}$ .<sup>4</sup>) However, it may be unnecessary to simulate a whole torus to reproduce small-scale, locally driven turbulence. In this paper we describe a coordinate system for nonlinear simulations that resolves a much smaller volume and is therefore computationally more efficient, while still resolving the relevant small scales. The smallest possible simulation volume is a long thin flux tube that is several correlation lengths wide in both perpendicular directions (radial and poloidal), and extended along the field line, exploiting the elongated nature of the turbulence ( $k_\perp \gg k_\parallel$ ). This approach is advantageous for fluid, gyrokinetic "Vlasov," and particle simulations, and could eventually be compared with full torus simulations.

The fundamental idea is to use coordinates that follow field lines. With such coordinates a flux tube (a tube with a surface parallel to  $\mathbf{B}$ ), which is bent by magnetic curvature and twisted by magnetic shear, is mapped into a rectangular domain. Such twisting coordinates were originally proposed by Roberts and Taylor,<sup>5</sup> and Cowley *et al.*<sup>6</sup> emphasized their utility for nonlinear calculations. In Ref. 7, we described the essential features of this approach, with an emphasis on slab geometry. Here we focus more on the toroidal aspects and actual details of implementation. The major problem of these field line coordinates is enforcing the periodicity constraint, since the coordinates are multivalued in a torus, except at low-order rational surfaces. In Ref. 6 it was emphasized that it is unlikely that the correlated volume wraps around the torus and overlaps itself. When this is true, the physical periodicity of the full torus is irrelevant, and the simplest approach is to simulate a flux tube subdomain that is several parallel correlation lengths long, just as it should be several perpendicular correlation lengths wide. As will be described in Sec. III, this can be different from imposing periodicity at  $\theta = \pm \pi$ , as is usually suggested for the ballooning representation, which could lead to artificial correlations and modify the results.

Another advantage of field-line coordinates, in addition to the efficiency of a minimum simulation volume, is that radial periodicity can be easily implemented, thus avoiding the problems of "quasilinear flattening" and allowing self-consistent turbulence-generated "zonal" flows (flows that cause flux surfaces to rotate). The field-line coordinates are also particularly convenient for gyrofluid simulations, where partially Fourier transformed quantities (in two of the three dimensions) need to be evaluated, such as  $|\omega_d(\theta)| \propto |k_\theta \cos(\theta) + k_r \sin(\theta)|$ .

In Sec. II we describe the general formulation of the basic geometry. The issues of periodicity and parallel boundary conditions are discussed in detail in Sec. III. Parallel boundary conditions for particle simulations are presented in Sec. IV. In Sec. V we discuss the relation of these flux tube coordinates to the standard ballooning transformation. We present some simulation results for toroidal ion temperature

<sup>a)</sup>Present address: Department of Physics, University of California, Los Angeles, Los Angeles, California 90024.

gradient (ITG) driven turbulence using this coordinate system in Sec. VI, and investigate the effect of the parallel boundary conditions. We have carried out simulations with various sizes for the flux-tube “box,” and verified that the results are independent of the box size once the box is larger than the correlation length in each direction, thereby justifying some of the assumptions implicit in simulating a flux tube subdomain rather than the full torus. This leads to interesting questions regarding Bohm versus gyro-Bohm scaling for the turbulence. In Sec. VII we discuss these results, the efficiency of flux tube simulation, and possible limitations of this approach. For completeness the equations used in the simulations are included in the Appendix. Reference 8 contains additional details and figures that may help the reader conceptualize these geometrical issues.

## II. FLUX TUBE SIMULATIONS IN GENERAL

If one wants to describe turbulence that is highly elongated along field lines and narrowly localized across field lines, it is natural to introduce coordinates that are constant on field lines. A natural way to do this for any general magnetic field is to use the Clebsch representation of the magnetic field<sup>9</sup> (since  $\nabla \cdot \mathbf{B} = 0$ ):

$$\mathbf{B} = \nabla \alpha \times \nabla \psi. \quad (1)$$

Clearly,  $\mathbf{B} \cdot \nabla \alpha = \mathbf{B} \cdot \nabla \psi = 0$ , so that  $\alpha$  and  $\psi$  are constant on field lines. Thus,  $\alpha$  and  $\psi$  are natural coordinates for the flux tube. A third coordinate,  $z$ , must be defined that represents distance along the flux tube. In many applications toroidal flux surfaces are defined, and it is natural to take  $\psi$  to be the poloidal flux. The choice of  $\alpha$  is less obvious and may be optimized for a particular calculation. A further complication is that  $\alpha$  and  $\psi$  are typically not naturally single valued and a cut must be introduced to enforce single values.<sup>9</sup> This issue will be discussed extensively below. Let us imagine that a choice of  $\alpha$ ,  $\psi$ , and  $z$  has been made and that  $\alpha = \alpha(\mathbf{r})$ ,  $\psi = \psi(\mathbf{r})$ , and  $z = z(\mathbf{r})$  are known functions, obtained, for instance, from an equilibrium code. Thus, the metric coefficients for the transformation to the  $\alpha, \psi, z$  coordinates are taken to be known.

We shall assume that the turbulence has short perpendicular correlation lengths compared to equilibrium scale lengths but a parallel correlation length on the order of the equilibrium scale lengths. Consider a flux tube simulation domain defined by  $\alpha_0 - \Delta\alpha < \alpha < \alpha_0 + \Delta\alpha$ ,  $\psi_0 - \Delta\psi < \psi < \psi_0 + \Delta\psi$ , and  $-z_0 < z < z_0$ . This volume is chosen to be several correlation lengths in all three directions, but should be as small as possible for computational efficiency. Once the box volume is larger than several correlation lengths, the turbulence should be insensitive to the size of the box. One tests whether the box size is adequate by increasing the box size and comparing the turbulence in the different size boxes, or by measuring the correlation functions in a given box and verifying that they go to zero at the edges of the box. In this way we arrive at a minimum simulation volume.

Three spatial operators appear many times in the equations for the perturbations  $\mathbf{B} \cdot \nabla$ ,  $\nabla_\perp^2$ , and  $\mathbf{B} \times \nabla \Phi \cdot \nabla$ . In the field-aligned coordinates  $x_i = (\alpha, \psi, z)$ , these are

$$\mathbf{B} \cdot \nabla A = (\nabla \alpha \times \nabla \psi \cdot \nabla z) \left( \frac{\partial A}{\partial z} \right)_{\alpha, \psi} = \frac{1}{J} \frac{\partial A}{\partial z}, \quad (2)$$

$$\nabla^2 A = \frac{1}{J} \sum_i \frac{\partial}{\partial x_i} \left[ J \left( \sum_j \frac{\partial A}{\partial x_j} \nabla x_j \right) \cdot \nabla x_i \right], \quad (3)$$

$$\mathbf{B} \times \nabla \Phi \cdot \nabla A = \sum_{i,j} \left( \frac{\partial A}{\partial x_j} \frac{\partial \Phi}{\partial x_i} \nabla x_i \times \nabla x_j \right) \cdot \mathbf{B}, \quad (4)$$

where  $A$  and  $\Phi$  are any scalars. Since the simulation volume is narrow in  $\alpha$  and  $\psi$  compared to equilibrium variations, all equilibrium quantities, or gradients of equilibrium quantities when they appear in these operators, are to lowest-order functions of  $z$  alone, with  $\alpha = \alpha_0$  and  $\psi = \psi_0$ . For example, the Jacobian  $J = (\nabla \alpha \times \nabla \psi \cdot \nabla z)^{-1}$  is to a good approximation constant across the box but not along the box, thus  $J = J(\alpha_0, \psi_0, z)$ . When  $A$  is a perturbed scalar ( $n, T$ , etc.), and  $\Phi$  is the electrostatic potential, we can neglect the  $\partial/\partial z$  terms in  $\nabla_\perp^2$ , and  $\mathbf{B} \times \nabla \Phi \cdot \nabla$ , since they are smaller by  $k_\parallel/k_\perp$ . Then, Eqs. (3) and (4) reduce to

$$\nabla_\perp^2 A = |\nabla \alpha|^2 \frac{\partial^2 A}{\partial \alpha^2} + 2 \nabla \alpha \cdot \nabla \psi \frac{\partial^2 A}{\partial \alpha \partial \psi} + |\nabla \psi|^2 \frac{\partial^2 A}{\partial \psi^2}, \quad (5)$$

$$\mathbf{B} \times \nabla \Phi \cdot \nabla A = \left( \frac{\partial A}{\partial \psi} \frac{\partial \Phi}{\partial \alpha} - \frac{\partial A}{\partial \alpha} \frac{\partial \Phi}{\partial \psi} \right) B^2. \quad (6)$$

Therefore, the equations to be solved in this minimum simulation volume have no explicit dependence on  $\alpha$  or  $\psi$ , which leads to great computational simplification. The  $\mathbf{E} \times \mathbf{B}$  nonlinearity takes the simple form Eq. (6), and all other coefficients in the equations are only functions of  $z$ .

The perpendicular boundary conditions on the perturbations at  $\alpha = \alpha_0 \pm \Delta\alpha$  and  $\psi = \psi_0 \pm \Delta\psi$  are taken to be periodic. If the box is more than a correlation length wide the turbulence should be insensitive to the boundary conditions, although one set of boundary conditions that is not advisable is fixed boundary conditions that prohibit energy and particle fluxes through the boundary. If fixed radial boundary conditions without sources or sinks are used, then the components of the perturbations that are constant on flux surfaces [the  $m=0, n=0$  components, i.e.,  $n(\psi)$ ,  $T(\psi)$ , where  $m$  and  $n$  are the poloidal and toroidal mode numbers] will grow to eventually cancel the driving equilibrium gradients (“quasilinear flattening”), thus turning off the turbulence. In principle, this problem can be overcome with a sufficiently large box so that the time scale to flatten the driving gradients becomes much longer than the simulation time, but periodic radial boundary conditions avoid flattening altogether and allow the use of a more efficient, smaller box. Past simulations have sometimes zeroed out the  $m=0, n=0$  components of perturbations to avoid this flattening, but this prevents the generation of sheared zonal  $\mathbf{E} \times \mathbf{B}$  flows resulting from the  $m=0, n=0$  component of  $\Phi(\psi)$ , which can be an important nonlinear saturation process.<sup>7,10–14</sup> Periodic radial boundary conditions allow the self-consistent evolution of  $m=0, n=0$  perturbations, such as the zonal flows.

The assumption of radial periodicity in the small flux tube is not based on actual physical constraints, which would

require simulating the full tokamak to include heating in the core, losses to the limiter or edge regions, etc. Instead, we are assuming that the statistical properties of the fluctuations at  $\psi+2\Delta\psi$  are the same as at  $\psi$ , and that if the simulation box width  $2\Delta\psi$  is larger than the radial correlation length we can assume that they are actually identical at every instant. Periodic boundary conditions are often used in two-dimensional plasma simulations or in simulations of homogeneous Navier–Stokes turbulence, but are complicated in three-dimensional plasma simulations by the shear in the magnetic field. The fluctuations tend to be elongated along the direction of the magnetic field, which points in different directions at different radii. In regular coordinates this requires the use of something like the “twist-and-shift” radial boundary conditions suggested by Kotschenreuther and Wong.<sup>10,15,16</sup> In coordinates already aligned with the magnetic field, however, radial periodicity becomes simply  $A(\psi+2\Delta\psi, \alpha, z, t) = A(\psi, \alpha, z, t)$ .

For the same reasons, we can also assume statistical periodicity in the  $\alpha$  direction,  $A(\psi, \alpha+2\Delta\alpha, z, t) = A(\psi, \alpha, z, t)$ . Since there is no explicit dependence of the operators in Eqs. (5) and (6) on  $\alpha$  or  $\psi$ , we use a Fourier series in  $\psi$  and  $\alpha$ , which also provides periodicity in those directions:

$$A(\psi, \alpha, z, t) = \sum_{j=-\infty}^{\infty} \sum_{k=-\infty}^{\infty} \hat{A}_{j,k}(z, t) \times e^{ij\pi(\psi-\psi_0)/\Delta\psi + ik\pi(\alpha-\alpha_0)/\Delta\alpha} \quad (7)$$

The boundary conditions in the  $z$  direction will be discussed in Sec. III. Note that while each term in the Fourier series is a plane wave in  $\alpha$ ,  $\psi$  coordinates, the wave fronts in real space can be very distorted, by magnetic shear, for example, measured by the parameter  $\hat{s} \equiv (r_0/q_0)(\partial q/\partial r)_{r=r_0}$ . Magnetic shear makes the angle between constant  $\alpha$  and  $\psi$  surfaces change as  $z$  changes—in real space the flux tube is then sheared and its cross section changes from a rectangle to a parallelogram. The wave fronts of each term in the Fourier series, Eq. (7), also get sheared. For example, the  $j=0, k \neq 0$  term has wave fronts corresponding to the constant  $\alpha$  lines. The individual terms in the series Eq. (7) are therefore “twisted eddies,”<sup>5,6</sup> whose wave fronts twist as one moves along  $z$ .

Now let us discuss the choice of the coordinates  $\alpha$  and  $\psi$ . As shown in Ref. 17, it is possible to choose  $\alpha$ ,  $\psi$ , and generalized “toroidal” and “poloidal” angle variables  $\zeta$  and  $\theta$ , such that the field lines are straight in the  $(\zeta, \theta)$  plane and physical quantities are periodic over  $2\pi$  in both variables. This choice of coordinates will simplify our discussion of periodicity in Sec. III. For the general magnetic field Eq. (1), we have<sup>9</sup>

$$\alpha = \phi - q(\psi)\theta - \nu(\psi, \theta, \phi), \quad (8)$$

where  $\psi = (2\pi)^{-2} \int_V d\tau \mathbf{B} \cdot \nabla \theta$  is the poloidal flux,  $q(\psi) = d\psi_T/d\psi$ ,  $\psi_T = (2\pi)^{-2} \int_V d\tau \mathbf{B} \cdot \nabla \phi$  is the toroidal flux,  $d\tau$  is the volume element, and  $\phi$  and  $\theta$  are the physical toroidal and poloidal angles, so physical quantities are peri-

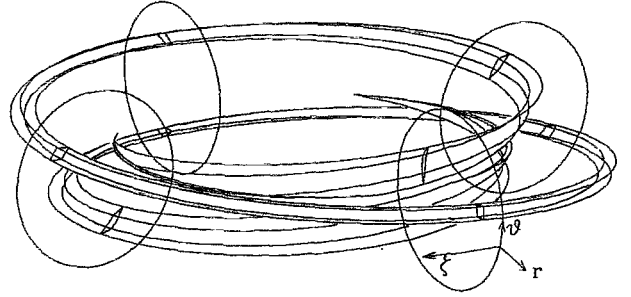


FIG. 1. The rectangular computational domain mapped onto a flux tube in a torus, with  $q_0=2.4$  and shear,  $\hat{s}=1.5$ . The ends of this flux tube are cut off at poloidal angle  $-\pi$  and  $\pi$ , and the sheared cross sections of the flux tube in the poloidal plane are indicated.

odic over  $2\pi$  in  $\phi$  and  $\theta$ . The function  $\nu$  is also periodic in  $\phi$  and  $\theta$ . We now introduce a new toroidal coordinate,  $\zeta = \phi - \nu(\psi, \theta, \phi)$ . With this choice,

$$\alpha = \zeta - q(\psi)\theta, \quad (9)$$

and the magnetic field lines are straight in the  $(\zeta, \theta)$  plane and are given by  $\alpha = \text{const}$ . Further, periodicity is preserved in  $\zeta$  and  $\theta$ . For our parallel coordinate  $z$  we will use  $z = \theta$ , since this makes our description very close to the usual ballooning mode formalism. Note that  $z$  is not restricted to  $-\pi < z < \pi$ , as we may choose to simulate a flux tube that wraps around the torus several times in the poloidal direction, not just once. This will be discussed further in Sec. III.

In summary, our field-line following coordinate system is given by  $(\psi, \alpha, z)$ , where field lines are labeled by constant  $\psi$  and  $\alpha$ . One can think of  $\psi$  as a radial coordinate,  $\alpha$  as a perpendicular-to-the-field coordinate, and  $z = \theta$  as a parallel-to-the-field coordinate. Our notation simplifies if we introduce the following new variables:

$$x = \frac{q_0}{B_0 r_0} (\psi - \psi_0), \quad y = -\frac{r_0}{q_0} (\alpha - \alpha_0), \quad z = \theta, \quad (10)$$

where  $q_0 = q(\psi_0)$ ,  $B_0$  is the field at the magnetic axis, and  $r_0$  is the distance from the magnetic axis to the center of the box. Then the representation of the perturbations, Eq. (7), becomes

$$A(x, y, z, t) = \sum_{k_x=-\infty}^{\infty} \sum_{k_y=-\infty}^{\infty} e^{ik_x x + ik_y y} \hat{A}_{k_x, k_y}(z, t), \quad (11)$$

with  $k_x = j\pi/\Delta x$ ,  $k_y = -k\pi/\Delta y$ ,  $\Delta x = q_0 \Delta\psi/B_0 r_0$ , and  $\Delta y = r_0 \Delta\alpha/q_0$ . The rectangular computational box of “radial” width  $2\Delta x$ , and “poloidal” width  $2\Delta y$ , and extended along the field line,  $\theta$ , is mapped onto a flux tube, as shown in Fig. 1, for example.

While Eqs. (2), (5), and (6) apply to general magnetic geometry, our simulations to date have used the traditional low- $\beta$ , large aspect ratio, concentric circular flux surface geometry. The specific forms of these operators then take the usual ballooning representation forms (see Ref. 8 for more details):

$$\hat{\mathbf{b}} \cdot \nabla A = \frac{1}{q_0 R_0} \frac{\partial A}{\partial \theta}, \quad (12)$$

$$\mathbf{v}_E \cdot \nabla A = \frac{c}{B^2} \mathbf{B} \times \nabla \Phi \cdot \nabla A = \frac{c}{B_0} \left( \frac{\partial \Phi}{\partial x} \frac{\partial A}{\partial y} - \frac{\partial \Phi}{\partial y} \frac{\partial A}{\partial x} \right), \quad (13)$$

and using the definition of  $\theta_0$  in Eq. (22),  $k_x = -k_y \hat{s} \theta_0$ ,

$$\nabla_{\perp}^2 A = -k_y^2 A [1 - \hat{s}^2 (\theta - \theta_0)^2]. \quad (14)$$

Toroidal terms enter through the magnetic drift frequency,  $\omega_d$ , which, using Eq. (4), is

$$\begin{aligned} i\omega_d A &= (cT/eB^2) \mathbf{B} \times \nabla B \cdot \nabla A \\ &= -ik_y A (cT/eB_0 R_0) [\cos \theta + \hat{s}(\theta - \theta_0) \sin \theta], \end{aligned} \quad (15)$$

for  $k_y \neq 0$ , and  $i\omega_d A = -ik_x A (cT/eB_0 R_0) \sin \theta$ , for  $k_y = 0$ .

These coordinates are similar to those used in Ref. 18. Our  $\alpha$ ,  $\psi$ , and  $z$  are analogous to  $-q\theta'$ ,  $\rho'$ , and  $\phi'$  in Ref. 18, respectively, since they have chosen to measure the distance along the field line with  $\phi'$ , a “toroidal” angle, while we use  $\theta$ . A more significant difference between our representation and Ref. 18 is the treatment of periodicity and the boundary conditions along the field line, though their more recent work<sup>19</sup> has adopted a similar treatment to ours, described in Sec. III.

### III. PERIODICITY AND PARALLEL BOUNDARY CONDITIONS

The choice of parallel boundary conditions involves a number of subtle, yet important, issues. The main concept is that of a statistically motivated periodicity, as described in Sec. II for the  $\psi$  and  $\alpha$  boundary conditions. For moderately “ballooning” turbulence we might expect parallel correlation lengths  $\theta_c \sim (1-2)\pi$  (though it might be longer than this). The simulation box should have a length  $2z_0 = 2\pi N$  in the parallel direction, which is several times the parallel correlation length. In some cases a box length of  $2\pi$  might be sufficient, but a longer box may be necessary to ensure that one end of the box is sufficiently decorrelated from the other end to avoid artificially constraining correlation effects, just as the box must be at least a few correlation lengths wide in the  $\psi$  and  $\alpha$  directions. For the cases simulated in Sec. VI, parallel box lengths of at least  $4\pi$  were needed for good convergence.

One must be careful about which other coordinates are held fixed while applying parallel periodicity, just as one must be careful to impose radial periodicity in field-line coordinates  $(\psi, \alpha, z)$  (i.e., impose periodicity in  $\psi$  while holding  $\alpha$  and  $z$  fixed), as discussed in Sec. II. Though the flux tube is rectangular in  $(\psi, \alpha)$  coordinates, it twists into a parallelogram in physical space as one follows the flux tube along  $z$ . The fluctuations in the physical plane perpendicular to a magnetic field line should be statistically identical at all places along that field line with the same poloidal angle ( $z = 0, 2\pi, 4\pi, \dots$ ), irrespective of the twisting of the flux tube, which increases without bound as  $z \rightarrow \infty$ . Because of this, we

will assume that the fluctuations are periodic in  $z$  while holding  $(\psi, \zeta)$  fixed, rather than holding the field-line coordinates  $(\psi, \alpha)$  fixed. Specifically, we impose

$$A[\psi, \alpha(\theta, \zeta), z(\theta)]|_{\theta=N\pi} = A[\psi, \alpha(\theta, \zeta), z(\theta)]|_{\theta=-N\pi},$$

or

$$A[\psi, \alpha(\theta + 2\pi N, \zeta), z(\theta + 2\pi N)] = A[\psi, \alpha(\theta, \zeta), z(\theta)]. \quad (16)$$

Physically, this is equivalent to considering two  $(\psi, \zeta)$  planes cutting through the flux tube, at  $z = \theta$  and at  $z = \theta + 2\pi N$ , and assuming that the turbulence is (statistically) identical in those two planes. To evaluate this periodicity constraint, first substitute  $\alpha = \zeta - q(\psi)\theta$ ,  $z = \theta$  into Eq. (7), and take  $\alpha_0 = 0$  for simplicity. Since the flux tube is thin, we can approximate  $q(\psi) \approx q_0 + (\psi - \psi_0)q'$ , where  $q' \equiv (dq/d\psi)_{\psi=\psi_0}$ , so Eq. (7) becomes

$$\begin{aligned} A &= \sum_{j=-\infty}^{\infty} \sum_{k=-\infty}^{\infty} \hat{A}_{j,k}(\theta, t) \\ &\times e^{i\pi(\psi - \psi_0)(j/\Delta\psi - kq' \theta/\Delta\alpha) + ik\pi\zeta/\Delta\alpha - ik\pi q_0 \theta/\Delta\alpha}. \end{aligned} \quad (17)$$

For convenience, we take the box width  $2\Delta\alpha$  to be  $1/n_0$  of the full toroidal circumference,

$$\Delta\alpha = \pi/n_0, \quad (18)$$

where  $n_0$  is a positive integer. Substituting this into Eq. (16) yields<sup>8</sup>

$$\hat{A}_{j+\delta j, k}(\theta + 2\pi N, t) C_k = \hat{A}_{j, k}(\theta, t), \quad (19)$$

where the phase factor  $C_k = \exp(-i2\pi N k q_0 n_0)$ ,

$$\delta j = 2\pi N k q' \Delta\psi/\Delta\alpha = 2n_0 k N \Delta q, \quad (20)$$

and  $2\Delta q = 2q' \Delta\psi$  is the change in  $q$  from one edge of the box to the other. Note that  $\delta j$  must be an integer, so  $J = 2n_0 N \Delta q$  must be an integer. This quantizes the range of  $q$  spanned by the flux tube, or the aspect ratio of the box,  $\Delta\psi/\Delta\alpha$  for  $q' \neq 0$ . One can treat shearless  $q' = 0$  cases as well, then  $\delta j = J = 0$ , and the radial box size  $2\Delta\psi$  is no longer quantized. In the usual  $q' \neq 0$  case, the radial position of the simulation box can be adjusted slightly so  $q_0$  is rational and  $C_k = 1$ .

Equation (19) thus expresses a modified periodicity condition on the mode amplitudes: the value of a coefficient at one end of the box is specified by the value of another coefficient with the same  $k$  but a different  $j$  at the other end of a box. Since computer simulations cannot retain an infinite set of  $j$ 's and  $k$ 's, enough  $j$  and  $k$  modes are kept to resolve up to a desired value of  $k_{\perp} \rho_i$ , above which the coefficients  $\hat{A}_{j,k}$  are assumed to vanish. Note that  $\delta j = 0$  for  $k = 0$  modes, so the periodicity condition for  $k = 0$  modes simplifies to  $\hat{A}_{j,0}(\theta + 2\pi N, t) = \hat{A}_{j,0}(\theta, t)$ .

This completes the formal specification of the boundary conditions, but we go on to express it in terms of notation often used in the ballooning transformation. It is common to introduce the “ballooning angle”  $\theta_0(j, k)$ , such that the radial derivative of an individual  $(j, k)$  mode of Eq. (17),

$$\frac{\partial}{\partial \psi} \bigg|_{\theta, \zeta} \propto i \pi \left( \frac{j}{\Delta \psi} - \frac{k q' \theta}{\Delta \alpha} \right), \quad (21)$$

vanishes at  $\theta = \theta_0$ . Note that this definition of  $\theta_0$  employs a derivative with respect to  $\psi$  while holding  $\theta$  and  $\zeta$  fixed, *not*  $\alpha$  and  $\theta$ . Clearly, at  $\theta = \theta_0(j, k)$  the wave fronts of the  $j$ , and  $k$ th term in Eq. (7) are perpendicular to the  $\psi$  surfaces. Equations (18) and (21) yield

$$k \theta_0(j, k) = \frac{j \Delta \alpha}{\Delta \psi q'} = \frac{j \pi}{n_0 \Delta q}. \quad (22)$$

Here  $\theta_0$  is discrete with spacing  $\delta \theta_0 = \pi / k n_0 \Delta q$ , which is dependent on  $k$ . Only the combination  $k \theta_0$  ever appears, and the limit  $k=0$  must be interpreted in terms of the discrete  $j$  sum. In particular, the turbulence can generate  $k=0$  ( $\theta_0 = \infty$ ) modes, corresponding to zonal flows that can be important in the nonlinear dynamics, so the  $k=0$  modes must be allowed to evolve self-consistently. Similar care must be taken in the shearless limit  $q'=0$ , where  $\theta_0 \rightarrow \infty$ . Using the definition of  $\theta_0$  in Eq. (22), we can express the shift  $\delta j$  in Eq. (20) as a shift in  $\theta_0$  instead:

$$\Delta \theta_0 = \frac{\delta j \pi}{k n_0 \Delta q} = 2 \pi N. \quad (23)$$

Using the definition of  $\theta_0$  to denote  $\hat{A}_{j,k}$  by a corresponding  $\hat{A}_{\theta_0,k}$ , and absorbing a phase factor that is independent of the coordinates  $(\psi, \theta, \zeta)$  by using  $\bar{A}_{j,k} = \hat{A}_{j,k} \exp\{-i k n_0 \times [q_0 \theta_0(j, k) + \alpha_0]\}$ , the parallel periodicity condition of Eq. (19) can be written as

$$\bar{A}_{\theta_0 + 2\pi N, k}(\theta, t) = \bar{A}_{\theta_0, k}(\theta - 2\pi N, t). \quad (24)$$

Using Eqs. (18) and (22) and  $q(\psi) \approx q_0 + (\psi - \psi_0) q'$  [or going back to Eq. (7) and using  $q$  itself for the radial-like coordinate  $\psi$ ], we can rewrite Eq. (17) as

$$A(\psi, \theta, \zeta, t) = \sum_{j=-\infty}^{\infty} \sum_{k=-\infty}^{\infty} \bar{A}_{j,k}(\theta, t) e^{i k n_0 \{\zeta - q(\psi) [\theta - \theta_0(j, k)]\}}. \quad (25)$$

It should be emphasized that Eqs. (17) and (25) are merely the same equations in different notation. Equation (25) bears a strong resemblance to the standard ballooning representation. There are, however, important differences that are discussed in Sec. V.

Equation (25), when used with the periodicity relation in Eq. (24), is periodic in  $\theta$  with period  $2\pi N$ . By setting  $N=1$ , this can satisfy physical periodicity in  $\theta$ , achieving the same result as the “sum over  $p$ ” in the standard ballooning representation. Thus, we are able to recover physical periodicity, as does the quasiballooning approach.<sup>16</sup> However, one should not necessarily use  $N=1$ . Rather, one should use a large enough  $N$  so that the parallel box length  $2z_0 = 2\pi N$  is at least several times the parallel correlation length. This point may be confusing, since  $\theta$  is a physical variable, periodic over  $2\pi$ . Of course, if we were simulating a full toroidal annulus with  $n_0=1$ , we should choose  $N=1$ . Indeed, Eq. (25) or (17) provides an expansion in a complete basis set if  $n_0=1$  and  $N=1$ . However, we are not trying to simulate a full toroidal annulus, but a thin flux tube whose width is only

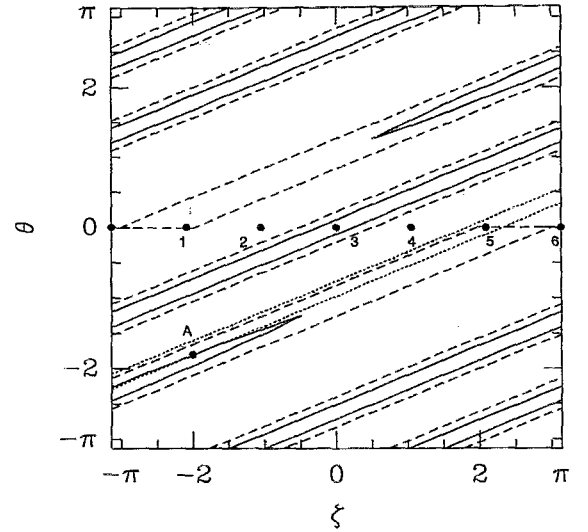


FIG. 2. Illustration on a flux surface of a possible correlated volume of the point 3 (enclosed by the solid line, with parallel correlation length  $\theta_c \approx 3\pi$ ), and a minimum simulation volume enclosed by the dashed line. The diagonal lines are parallel to the field lines (here  $q=2.4$ ). In this case the simulation volume has a toroidal width of one-sixth the total toroidal circumference, i.e.,  $n_0$  in Eq. (18) is 6. If the potential is represented by Eq. (25) and  $\Phi$  is made periodic in  $\theta$ , there are six identical copies of the correlated volume centered at the points 1–6. The correlated volume of point 5 (dotted line) partially overlaps the correlated volume of point 3, at the point marked A. This is unphysical and can be avoided in this case by making the system periodic over  $4\pi$ ,  $-2\pi < \theta < 2\pi$ . The minimum simulation volume illustrated is for  $-2\pi < \theta < 2\pi$ .

$1/n_0$  of the full toroidal circumference. Then, Eq. (25) represents  $n_0$  identical copies of the simulation volume if one considers the full range of  $\zeta$ ,  $0 \rightarrow 2\pi$ . Following the flux tube along the field lines (at fixed  $\alpha$ ) from  $\theta=0$  to  $\theta=2\pi$  will not lead to the same physical location (unless  $q$  is an integer) but to one of the  $n_0-1$  identical copies of itself. Forcing periodicity at this point is undesirable (unless the parallel correlation length is indeed significantly shorter than  $2\pi$ ), because it is a fiction of simulating only  $1/n_0$  of the toroidal direction with  $n_0$  identical copies.

This is illustrated by Fig. 2, which shows a correlated volume with a parallel correlation length  $\theta_c \approx 3\pi$ , and a perpendicular correlation length equal to half the simulation box width,  $\alpha_c = \Delta \alpha = \pi/6$ . If the simulation box has a parallel length of only  $2\pi$ , this correlated volume would be forced to overlap with one of the  $n_0$  images of itself, causing artificial interference effects. By extending the simulated flux tube to a length of  $4\pi$ , we allow the whole region to evolve self-consistently.

Of course, at an integer  $q$  flux surface, a simulation volume really does overlap itself within a distance  $\theta=2\pi$  and experience these interference effects. More generally, a correlated volume will overlap itself when  $\theta$  increases by  $2\pi N$  if  $q 2\pi N \bmod 2\pi$  is less than the perpendicular correlation length  $\alpha_c$ . This can be used to define a maximum parallel length  $\theta_{\max}$ , which the flux tube can be without physically overlapping itself. Here  $\theta_{\max}$  is also the maximum correlation length a correlated perturbation can have without “biting its tail” and experiencing coherent interference effects. In addi-

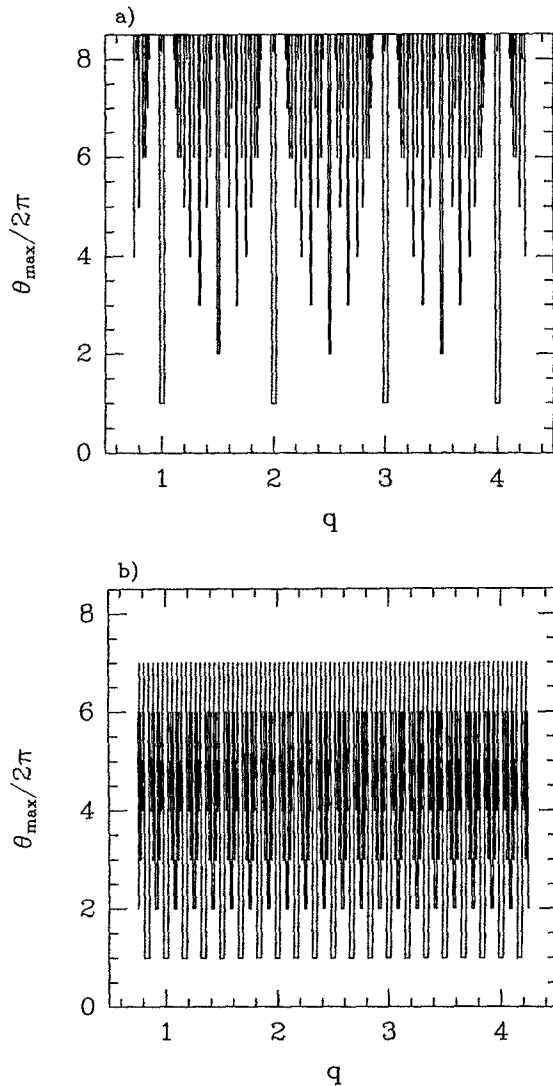


FIG. 3. Distance along the field line,  $\theta_{\max}$ , at which a correlated volume (with perpendicular width  $2\Delta\alpha=\pi/25$ ) overlaps itself, for varying  $q$ . (a) For  $n_0=1$ ,  $\theta_{\max}$  is small only near low-order  $q$  surfaces. (b) For  $n_0=6$ , the maximum correlation length is reduced, since the correlated volume can hit copies of itself. In this case, if the physical correlation length is longer than  $\theta_{\max}$ , the box must be extended and the periodicity condition relaxed.

tion,  $\theta_{\max}$  is plotted versus  $q(\psi)$  in Fig. 3. Note that if one simulates only  $1/n_0$  of the toroidal direction, then a correlated perturbation is  $n_0$  times as likely to run into itself or one of its images. In this case we may need to extend the parallel length of the simulated flux tube to avoid these artificial correlations. For most of the plasma, there is no difficulty in extending the simulated flux tube to be two to three times longer than  $2\pi$ , without having the flux-tube physically run into itself. Even for a simulation flux tube that spans a range of  $q$  values, for example,  $2\Delta q \sim \frac{1}{2}$ , at worst the flux tube might overlap itself briefly near an integer or half-integer  $q$  surface. As pointed out in Ref. 6, these low-order rational surfaces occupy a small fraction of a minor radius of a tokamak, and so it is very infrequent that a correlated perturbation will “bite its tail.” Furthermore, experimental evidence<sup>20</sup> on tokamaks indicates that there are no unusual

features near low-order rational surfaces, except when there are macroscopic MHD instabilities.

In practice, we find that the flux-tube length  $2\pi N$  does not need to be extremely large, and  $N=2$  may usually be sufficient. For the particular cases in Sec. VI, we find that  $N=1$  simulations produce a  $\chi_i$  that is about 30% low, while  $N=2-4$  are virtually indistinguishable. However, there may be other cases where an even larger  $N$  is required. In each case, one should justify the value of  $N$  *a posteriori*, by verifying that the parallel correlation functions from the simulations indeed fall off significantly in a distance  $2\pi N$ , and/or by carrying out convergence studies with different values of  $N$ , as in the perpendicular directions.

We have also tested different parallel boundary conditions. Instead of imposing parallel periodicity holding  $\psi$  and  $\zeta$  fixed, Eq. (16), the perturbations could simply be zeroed,  $A(\psi, \alpha, z = \pm\pi N) = 0$ , or we could impose periodicity in  $z$  at fixed  $\psi$  and  $\alpha$ . While these two alternate boundary conditions should give the same result as our proposed method, Eq. (16), as the box length becomes very long, they do not converge as rapidly. We will concentrate on the case where periodicity in  $z$  is imposed at fixed  $\psi$  and  $\alpha$ , so  $A(\psi, \alpha, +\pi N) = A(\psi, \alpha, -\pi N)$ , and each  $A_{j,k}$  mode in Eq. (7) is periodic with itself at  $z = \pm\pi N$ . In this case, every field line is effectively a rational field line that connects to itself, since particles flowing out one end of the box flow back in the other end on the same field line. This is unlike a real sheared magnetic field, where most field lines are irrational and never connect to themselves. This is particularly important for electron dynamics, since electrons move rapidly along the field lines, and have time to sample a large fraction of the flux surface if  $q$  is irrational. When using the condition  $A(\psi, \alpha, +\pi N) = A(\psi, \alpha, -\pi N)$  for the ions, we therefore distinguish between two ways of treating the electrons: treating  $q$  as rational everywhere for electrons, and treating  $q$  as irrational everywhere for electrons. If  $q$  is irrational, the field line average  $\langle\Phi\rangle$  in the adiabatic electron response,  $n_e = \Phi - \langle\Phi\rangle$  (see the Appendix), is a flux surface average, and is zero unless  $k_y = 0$ . If  $q$  is made rational everywhere, the field line average  $\langle\Phi\rangle$  is a function of  $\alpha$ , and is nonzero for  $k_y \neq 0$  modes, changing the quasineutrality constraint. This drastically changes the linear growth rates, and consequently, the turbulent heat flux. For the low shear cases in Sec. VI, the heat flux increases by a factor of 7.

Even if we treat  $q$  as irrational for the adiabatic electron response, which is more realistic, using periodicity at fixed  $(\psi, \alpha)$  for the ions yields heat diffusivities of  $(7.8, 4.5, 7.5)\rho_i^2 v_{ti}/L_n$  for box lengths  $(2, 4, 6, 8)\pi$ , respectively, for the low shear cases in Sec. VI, while our approach converged to  $5\rho_i^2 v_{ti}/L_n$  at a box length of only  $4\pi$ . The alternate boundary conditions converge more slowly because the ends of the box are wasted by not smoothly connecting the turbulence at each end. Specifically, using  $A(\psi, \alpha, +\pi N) = A(\psi, \alpha, -\pi N)$  causes discontinuities in the spatial gradient operators for a given  $k_y$  and  $\theta_0$  mode across the ends of the box. For example, at  $\theta = \pi N$ ,  $\nabla_{\perp}^2 A = -k_y^2 A_{j,k}(\pi N)[1 + \hat{s}^2(\pi N - \theta_0)^2]$ , while at  $\theta = -\pi N$ ,  $\nabla_{\perp}^2 A = -k_y^2 A_{j,k}(-\pi N)[1 + \hat{s}^2(-\pi N - \theta_0)^2]$ , which is different if  $\theta_0 \neq 0$ . This distorts the eddies and damps the turbulence near the ends of the box. If the



ends are in the good curvature regions (lengths of  $2\pi$ ,  $6\pi$ ) the flux is high, and if the ends are in the bad curvature regions ( $4\pi, 8\pi$ ) the flux is low. Our boundary condition Eq. (24) connects  $A_{j,k}(\pi N)$  to another mode with  $\theta_0$  shifted by  $2\pi N$  to make the spatial operators continuous.

#### IV. BOUNDARY CONDITIONS FOR PARTICLE SIMULATIONS

Particle simulations can also take advantage of an optimum flux-tube simulation volume using the field-line coordinates  $(\psi, \alpha, z)$  described in Sec. II. Field quantities such as the electrostatic potential can be represented by the Fourier series, Eq. (7), with the parallel boundary conditions given by Eq. (19), or equivalently, Eq. (24). For the particles, we must specify the location where a particle will reenter the box after passing through an edge of the box. The particle's velocity should not be changed. In the perpendicular directions,  $\psi$  and  $\alpha$ , standard periodicity is used. In the parallel direction, we apply Eq. (16). Using  $\alpha = \zeta - q(\psi)\theta$  and  $z = \theta$ , we see that if a particle exits the box at the position  $(\psi_1, \alpha_1, z = +\pi N)$ , where  $\alpha_1 = \zeta_1 - q(\psi_1)\pi N$ , then it will reenter the opposite side of the box at  $(\psi_2, \alpha_2, z = -\pi N)$ , where  $\psi_2 = \psi_1$ , and  $\alpha_2 = \zeta_1 + q(\psi_1)\pi N$ . Thus, the particle will be shifted in  $\alpha$  by the amount

$$\delta\alpha = \alpha_2 - \alpha_1 = q(\psi_1)2\pi N \bmod 2\Delta\alpha, \quad (26)$$

where the modulo operation accounts for the fact that if this shift in  $\alpha$  causes  $\alpha_2$  to fall outside the range of the box,  $-\Delta\alpha < \alpha < \Delta\alpha$ , then the particle has fallen into a periodic copy of the original box, and is simply shifted by a multiple of  $2\Delta\alpha$  back into the simulation domain. Expanding  $q(\psi)$ , using Eqs. (18) and (19), and introducing an integer  $K$  to reproduce the modulo function, we find

$$\frac{\delta\alpha(\psi)}{2\Delta\alpha} = q_0 N n_0 + K + J \frac{(\psi - \psi_0)}{2\Delta\psi}. \quad (27)$$

At the outer edge of the box,  $\psi = \psi_0 + \Delta\psi$ , the box has twisted by  $J/2$  box lengths in the  $\alpha$  direction, and by  $-J/2$  box lengths at the inner edge of the box,  $\psi = \psi_0 - \Delta\psi$ . Thus,  $J$  represents the integer number of box widths in  $\alpha$  that the box has twisted from one end in  $z$  to the other end. This is illustrated for  $J=2$  in Fig. 4. In this figure,  $q_0 N n_0$  is assumed to be an integer for simplicity, so the center of the box is at the same physical point at  $\theta = \pm\pi N$ . In general, the ends of the box will overlap with periodic copies of the original box.

To summarize, if a particle leaves the box from  $(\psi_0 + \Delta\psi, \alpha, z)$  then it reenters at  $(\psi_0 - \Delta\psi, \alpha, z)$ ; if it leaves from  $(\psi, +\Delta\alpha, z)$  then it reenters at  $(\psi, -\Delta\alpha, z)$ ; and if it leaves from  $(\psi, \alpha, +\pi N)$  it reenters at  $(\psi, \alpha + \delta\alpha, -\pi N)$ . All of the above boundary conditions are reversible, i.e., if a particle leaves at  $(\psi - \Delta\psi, \alpha, z)$  it will reenter at  $(\psi + \Delta\psi, \alpha, z)$ , etc. More details on the implementation of boundary conditions for particle simulations are given in Ref. 8.

#### V. THE BALLOONING TRANSFORMATION AND ITS RELATION TO FLUX-TUBE SIMULATION

The linear theory of short perpendicular wavelength instabilities in tokamaks has been developed largely in terms

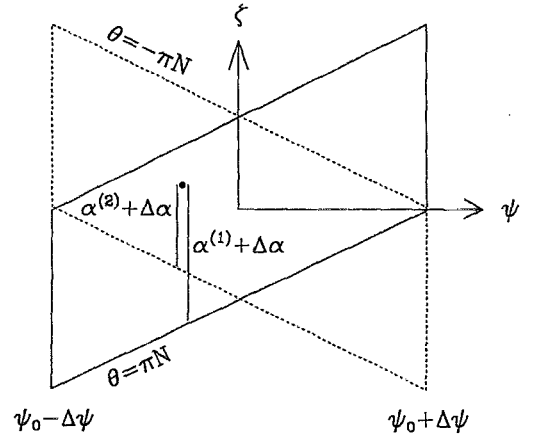


FIG. 4. Boundary conditions in the parallel direction for particle simulations. At  $\theta=0$ , the simulation box is rectangular in  $\zeta$  and  $\psi$ . The twisted ends of the box at  $\theta=\pi N$  (solid) and  $\theta=-\pi N$  (dashed) are shown. If a particle leaves the  $\theta=\pi N$  end of the box at  $\alpha^{(1)}$ , it reenters the  $\theta=-\pi N$  end of the box at  $\alpha^{(2)}$ , given by Eq. (26).

of the so-called “ballooning transformation.”<sup>21</sup> In this section we will discuss the relationship of the “ballooning transformation” to our flux tube simulation scheme. In ballooning theory a single eigenmode is represented as

$$\Phi_n(\psi, \theta, \zeta, t) = \sum_{p=-\infty}^{\infty} e^{-i\omega t + i n \zeta - i n q(\psi)(\theta - \theta_0 + 2\pi p)} \times \hat{\Phi}_{n, \theta_0}(\theta + 2\pi p, \psi), \quad (28)$$

where  $\theta_0 = \theta_0(\psi)$  and  $\hat{\Phi}_{n, \theta_0}(\theta, \psi)$  depend on  $\psi$ . The toroidal mode number  $n$  is any large integer. The variation in  $\theta$  and  $\psi$  of the exponential is large, whereas the variation of  $\theta_0$  and  $\hat{\Phi}$  is finite. In lowest order in an expansion in  $1/nq$  one obtains a differential equation in  $\theta$  for  $\hat{\Phi}_{n, \theta_0}(\theta, \psi)$ . This equation is solved with  $\theta_0$  a parameter and with the boundary conditions  $\hat{\Phi} \rightarrow 0$  as  $|\theta| \rightarrow \infty$ , so the sum over  $p$  can converge. Periodicity in  $\theta$  is recovered by the  $p$  summation in Eq. (28). A lowest-order approximation to the eigenvalue  $\omega_n(\theta_0, \psi)$  is obtained on each surface. In higher order, the eigenvalue is quantized by solving radial differential equations. Much has been written about this higher-order procedure to find the radial behavior, and we cannot do justice to the subtleties here.<sup>22</sup> Let us consider instead a narrow radial annulus  $\psi_0 - \Delta\psi < \psi < \psi_0 + \Delta\psi$ . Let  $\Phi$  be periodic in  $\psi$  over  $2\Delta\psi$  at constant  $\alpha = \zeta - q(\psi)\theta$  and  $\theta$ , then we can represent the radial variation of  $\Phi$  in a Fourier series in  $\psi$ ; with  $n\theta_0 = l\pi/\Delta q$ , i.e., the  $\psi$  variation of  $\theta_0(\psi)$  and  $\hat{\Phi}_{n, \theta_0}(\theta, \psi)$  are combined into a discrete series in  $\theta_0$ . Thus, one could write for an arbitrary perturbation in this annulus:

$$\Phi(\psi, \theta, \zeta, t) = \sum_{n=-\infty}^{\infty} \sum_{l=-l_0+1}^{l_0} \sum_{p=-\infty}^{\infty} e^{i n \zeta - i n q(\psi)(\theta + 2\pi p) + i l \pi (\psi - \psi_0)/\Delta\psi} \times \tilde{\Phi}_{n, l}(\theta + 2\pi p, t), \quad (29)$$



where we have rescaled  $e^{ilq_0\pi/q'\Delta\psi}\hat{\Phi}_{n,l} = \bar{\Phi}_{n,l}$ . The  $p$  summation makes this expression manifestly periodic in  $\theta$ . Expanding  $q(\psi)$ , so  $\exp[-inq_0\pi p + il\pi(\psi - \psi_0)/\Delta\psi] = \exp[-inq_0\pi p + i\pi(l - 2pn)\Delta q(\psi - \psi_0)/\Delta\psi]$ , it is clear that in this summation we need only take  $|l| \leq l_0 = n\Delta q$ , since otherwise the  $p$  and  $l$  sums duplicate terms. This restricts the bandwidth in  $\psi$  of the perturbations in ballooning space, and makes the ballooning transformation unique.<sup>23</sup>

If we set  $n_0=1$  in Eq. (25) and  $N=1$  in Eq. (19) we obtain an exactly equivalent representation to Eq. (29). To see this, we note that the  $j$  in Eq. (25) and  $p$  and  $l$  in Eq. (29) are related by  $j=l-2pl_0$  and  $\delta j=2l_0$ , and we set  $k=n$ . Thus, the  $-\pi < \theta < \pi$  range of the  $\bar{\Phi}_{n,l}$  modes with  $|l| < l_0$  correspond to the  $\bar{A}_{j,k}$  modes with  $|j| < \delta j/2$  (defined only from  $-\pi < \theta < \pi$  for  $N=1$ ). The  $\bar{A}_{j,k}$  modes with  $|j| > \delta j/2$  correspond to the  $-\pi - 2\pi p < \theta < \pi - 2\pi p$  range of the  $\bar{\Phi}_{n,l}$  modes with  $p = (j-l)/\delta j$ . The boundary condition Eq.

(19) makes this series of  $\bar{A}_{j,k}$  modes (for all  $j$ ) identical to  $\bar{\Phi}_{n,l}$  (for  $|l| < l_0$ ) defined on the extended domain  $-\infty < \theta < \infty$  (when  $n_0=N=1$ ).

Using the boundary condition, Eq. (19), and a finite  $\theta$  range simplifies the evaluation of the  $\mathbf{E} \times \mathbf{B}$  nonlinearities compared to the usual ballooning representation. The simple form, Eq. (6), is easy to evaluate using a pseudospectral method. A fully spectral method remains in  $\mathbf{k}$  space at all times, so the nonlinear terms become convolutions in  $\mathbf{k}$  space and require of order  $N_x^2 N_y^2 N_z \sim N^5$  operations. By using fast Fourier transforms (FFT's), the pseudospectral method reduces the operations to  $N_x N_y N_z (\log_2 N_x + \log_2 N_y) \sim N^3$ , resulting in a very significant savings for large  $N$ .

In the ballooning representation [i.e., using Eq. (29) to represent the perturbations], the nonlinear terms involve sums over  $p$ :<sup>24</sup>

$$(\mathbf{v}_E \cdot \nabla \mathbf{A})_{n,l}(\theta) = \frac{c}{2} \sum_{n'+n''=n} \sum_{l'} \sum_{p',p''} e^{-2\pi i q_0(n'p' + n''p'')} n' n'' q' [2\pi(p'' - p') + \theta'_0 - \theta''_0] \\ \times [\bar{\Phi}_{n',l'}(\theta + 2\pi p') \bar{A}_{n'',l''}(\theta + 2\pi p'') - \bar{A}_{n',l'}(\theta + 2\pi p') \bar{\Phi}_{n'',l''}(\theta + 2\pi p'')], \quad (30)$$

where  $l'' = l - l' + 2\Delta q(n'p' + n''p'')$  and  $\theta_0(n,l) = l\pi/n\Delta q$ . Again,  $|l'| \leq |n'|\Delta q$  and  $|l''| \leq |n''|\Delta q$ , and  $\bar{A}$  and  $\bar{\Phi}$  are defined on an infinitely extended  $\theta$  domain, without the boundary condition, Eq. (19). This expression differs slightly from earlier literature since we are using a discrete representation in  $\psi$ , and have implicitly used the inverse ballooning transformation.<sup>23</sup> If the mode width in  $\theta$  is less than  $\pi$ , the sums over  $p$  appear to be a small effect, and are usually neglected in nonlinear calculations using the ballooning representation. This conclusion may be misleading. Noting that in Eq. (29),  $k_x = j\pi/\Delta x = (l - 2pl_0)\pi/\Delta x$  and  $k_y = -n\pi/\Delta y = -nq_0/r_0$ , we see that in the standard ballooning representation, only a wedge of  $\bar{\Phi}_{n,l}$ 's in  $(k_x, k_y)$  space are evolved,  $-n\Delta q < l < n\Delta q$  (for  $n \neq 0$ ), and the rest of  $\mathbf{k}_\perp$  space is filled by the sum over  $p$ . For small  $n$ , the evolved range of  $k_x$ 's is small, so it may take many terms in the  $p$  sum to reach moderate  $k_x$ 's. The evolved wedge of  $k_x$  modes corresponds to a wedge of  $\theta_0$ 's from  $-\pi < \theta_0 < \pi$ . In our representation, since we evolve a rectangular grid in  $\mathbf{k}_\perp$  space, the  $\theta_0$  range is not limited to  $|\theta_0| < \pi$ . The nonlinear interaction between a mode  $(k_x, k_y)$  within the  $p=0$  wedge and a mode outside the wedge could be strong, even if its linearly most unstable mode structure (of many eigenmodes in  $\theta$ ) is centered a long distance down the field line. For low  $k_y$  and large  $k_x$  one would have to include many  $p$ 's to capture this interaction. In our nonlinear simulations, we do see modes outside the  $p=0$  wedge excited to significant amplitudes. While the form of the  $\mathbf{E} \times \mathbf{B}$  nonlinearity in Eq. (6) can be efficiently evaluated with FFT's, it is not obvious that Eq. (30) can be. However, since our representation is equivalent to the ballooning representation (if  $n_0=N=1$ ), it automatically includes the sums over  $p$  in the nonlinearity. Our rep-

resentation should also be more convenient for analytic calculations, since the nonlinearity takes a simple form, and the choice of  $\theta_0$ 's, or  $k_x$ 's, is well defined.

## VI. SIMULATION RESULTS

We have implemented this coordinate system in nonlinear gyrofluid simulations of toroidal ITG turbulence. The simulation results are presented here to describe practical computational issues and to test some of our assumptions. It is not meant to be a complete description of our gyrofluid equations or our nonlinear results, which are discussed in Ref. 8. Therefore, we have relegated the actual equations to the Appendix.

There are some subtleties involving the implementation of the boundary condition, Eq. (19), because our equations involve  $|k_\parallel|$  Landau damping terms (equivalent to a nonlocal integral operator in real space<sup>25</sup>). Two separate methods for implementing this boundary condition are described in detail in Ref. 8, which we refer to as the "equal-length extension" and "multiply connected" methods. In practice, we have observed no significant differences between these methods in the nonlinear simulations done to date. These issues are ignorable for a particle or Vlasov simulation, since they do not require evaluation of  $k_\parallel$  and can directly use the boundary conditions in Sec. IV.

To test the small-scale assumption, we present two simulations: one with perpendicular dimensions ( $L_x = 85\rho_i$ ,  $L_y = 100\rho_i$ ), and one with double the box size ( $L_x = 170\rho_i$ ,  $L_y = 200\rho_i$ ). That these simulations give similar results indicates that the small flux tube may be capturing the essence of the turbulence. It is a necessary but not sufficient test, as discussed in Sec. VII. The physical parameters are taken

from the Tokamak Fusion Test Reactor<sup>26</sup> (TFTR) L-mode shot #41309:  $\eta_i=4$ ,  $L_n/R=0.4$ ,  $\hat{s}=1.5$ ,  $q=2.4$ ,  $T_i=T_e$ ,  $\rho_i=0.14$  cm,  $L_n=103$  cm, and the computational box is centered at  $r_0=53$  cm. The box sizes then correspond to  $n_0=10$  for the small box and  $n_0=5$  for the large box. Both simulations use 64 grid points along the field line coordinate  $\theta$ . Using 128 grid points along  $\theta$  gives essentially the same results. For these runs,  $N=2$ , so the physical  $\theta$  domain extends from  $-2\pi$  to  $2\pi$ . The equal length ( $\pi$ ) extension method (for a total extended  $\theta$  domain from  $-3\pi$  to  $3\pi$ ) was used to implement the parallel boundary condition.

We use a spectral representation in  $x$  and  $y$ , with  $\pm 42k_x$  modes and  $\pm 15k_y$  modes for the small simulation and  $\pm 63k_x$  modes and  $\pm 21k_y$  modes for the large simulation, not counting additional modes added at high  $k$  for dealiasing. The modes are evenly spaced such that  $k_y^{\max}\rho_i \approx 1$  and  $k_x^{\min} \approx k_y^{\min}$ , making the computational domain roughly square in  $x$  and  $y$ . For  $N>1$ , it is necessary to include more  $k_x$ 's to include unstable modes localized near  $\theta=\pm 2\pi$ ,  $\pm 4\pi$ , etc., in the bad curvature regions (i.e., modes with  $\theta_0$ 's near  $\pm 2\pi$ ,  $\pm 4\pi$ , etc.). The modes tend to be localized along the field line near  $\theta_0$ , so ideally one would like to include enough  $k_x$ 's to cover the range  $-\pi N < \theta_0 < \pi N$  for all  $k_y$ 's. This is very expensive at high  $k_y$ , where the spacing in  $\theta_0$  gets small, since  $\theta_0 = -k_x/\hat{s}k_y$ . We arrange our modes in  $k$  space so that the  $\theta_0$ 's cover the  $\theta$  domain for low  $k_y$ 's, but not high  $k_y$ 's. This implies  $k_x^{\max} \gg k_y^{\max}$  for  $N>1$  and  $\hat{s}\approx 1$ . Since most of the energy is at  $k_y\rho_i < \frac{1}{2}$ , the missing  $\theta_0$ 's at high  $k_y$  have a very little effect.

Figure 5 shows contours of electrostatic potential in the  $(x,y)$  plane at  $\theta=0$  (the outer midplane of the torus), for both runs at saturation. (The fluctuations on the inner midplane have roughly one-half the amplitude, which would be an interesting feature to look for in experiments.) It is apparent that although the box was doubled, the dominant scale did not change. This is also evident from the spectra in Fig. 6, also at  $\theta=0$ , where  $|\Phi|^2(k_x) = \sum_{k_y} \Phi_{k_x,k_y} \Phi_{k_x,k_y}^*$ ,  $|\Phi|^2(k_y) = \sum_{k_x} \Phi_{k_x,k_y} \Phi_{k_x,k_y}^*$ , and the low resolution spectra are reduced by a factor of two to account for mode density. Although the resolution has increased, the shape and the location of the peak in the spectrum is roughly the same. These spectra are similar to BES measurements on TFTR.<sup>1</sup> The large  $k_y=0$  component is evidence of sheared zonal  $\mathbf{E}\times\mathbf{B}$  flows,<sup>7</sup> which are primarily in the poloidal direction. Though there are some small differences in the spectra, the two runs agree within statistical fluctuations on global quantities such as the volume-averaged RMS fluctuation levels and transport levels:  $e\Phi/T_i = 15\rho_i/L_n \approx 0.020$  and  $\chi_i = 7.4\rho_i^2 v_{ti}/L_n$ , averaged from  $tv_{ti}/L_n = 150-300$ . The statistical fluctuations in  $\chi_i$  at saturation are about 10% for both runs. This level of ion heat transport is near the experimentally measured  $\chi_i = 8.8\rho_i^2 v_{ti}/L_n$ , but these simulations ignore impurities and beams (usually a stabilizing effect), trapped electrons (destabilizing), and use our four moment model, which gives lower transport than our more accurate six moment model. Nevertheless, this level of agreement is encouraging, and suggests that toroidal ITG turbulence is responsible for anomalous ion heat transport in tokamaks. The transport

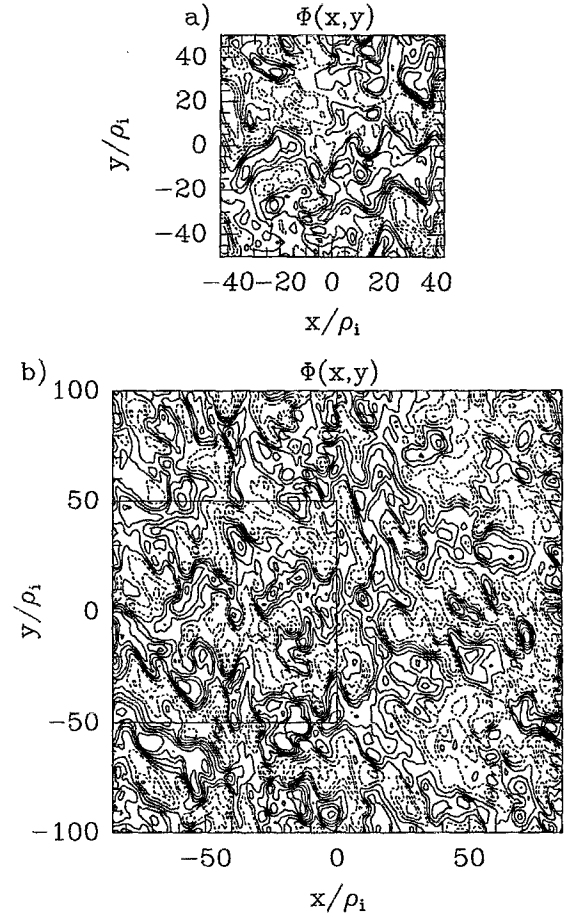


FIG. 5. Contours of potential for (a) a small run and (b) a large run. Doubling the perpendicular simulation domain did not change the dominant scale of the fluctuations.

from these toroidal simulations is about a factor of 25 larger than sheared slab simulations for the same parameters, demonstrating the importance of toroidicity. Our toroidal simulations can be run in the sheared slab limit by taking  $L_n/R \rightarrow 0$  and  $q/\hat{s} \rightarrow 0$ , so that  $L_n/L_s = L_n\hat{s}/qR$  remains finite. We should point out that our preliminary results, Fig. 2(a) of Ref. 7, were high by a factor of  $\frac{16}{3}$ , due to a numerical error in calculating  $\chi_i$ . The remaining change is due to increased resolution.

We have also performed tests varying the box length in the parallel direction. For these tests we have used the “multiply connected” method to implement the parallel boundary conditions, for greatest accuracy, as described earlier in this section. Figure 7(a) shows the time evolution of the volume-averaged  $\chi_i$  for two runs with box length  $N=1$  and 2, i.e.,  $\Delta\theta=2\pi$  and  $4\pi$ , with  $n_0=10$ , and other parameters as above. Figure 7(b) shows the correlation function along the field line,

$$C(\theta, 0) = \frac{\langle \Phi(x, y, \theta) \Phi(x, y, \theta=0) \rangle}{\langle \Phi(x, y, \theta=0)^2 \rangle}, \quad (31)$$

for the two runs. The averaging  $\langle \rangle$  is over  $x, y$ , and time once the simulation has reached a quasisteady state. If this correlation function were not averaged in  $x$  and  $y$  (only taken

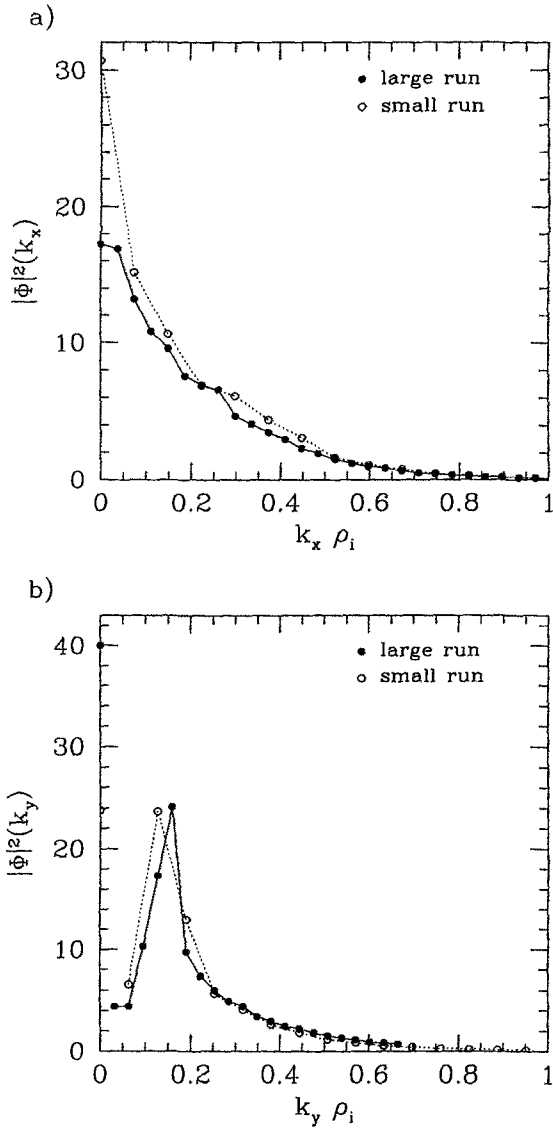


FIG. 6. Potential spectra for both runs.

along the field line passing through  $x=y=0$ ), it would return to one at  $\theta=\pm 2\pi$  for the  $N=1$  run, because of periodicity. The Fourier transform of  $C(\theta,0)$  is the  $k_{\parallel}$  spectrum. As discussed in Sec. III, since  $n_0 > 1$ , using a box with  $-\pi < \theta < \pi$  ( $N=1$ ), can artificially constrain the parallel correlation length. There are significant correlations at  $\theta \pm \pi$  for these parameters, indicating that this is the case, and that the box should be extended. These additional correlations in the  $2\pi$  box are in some way constraining the nonlinear dynamics and reducing the flux.

It is easier to test the scaling with box length at low shear, since the turbulence at  $\pm 2\pi$ ,  $\pm 4\pi$ , etc., is not at such high  $k_x$ , because  $k_x = -k_y \hat{s} \theta_0$ . This allows resolution of the turbulence along the entire box length with fewer  $k_x$  modes than at high shear. Also, at low shear the linear mode structure is broader in  $\theta$ , leading to slightly broader parallel correlation functions. Figure 8(a) shows the time evolution of  $\chi_i$  in four runs with box lengths  $N=1,2,3,4$  or  $\Delta\theta = 2\pi, 4\pi, 6\pi, 8\pi$ . The physical parameters are the same as

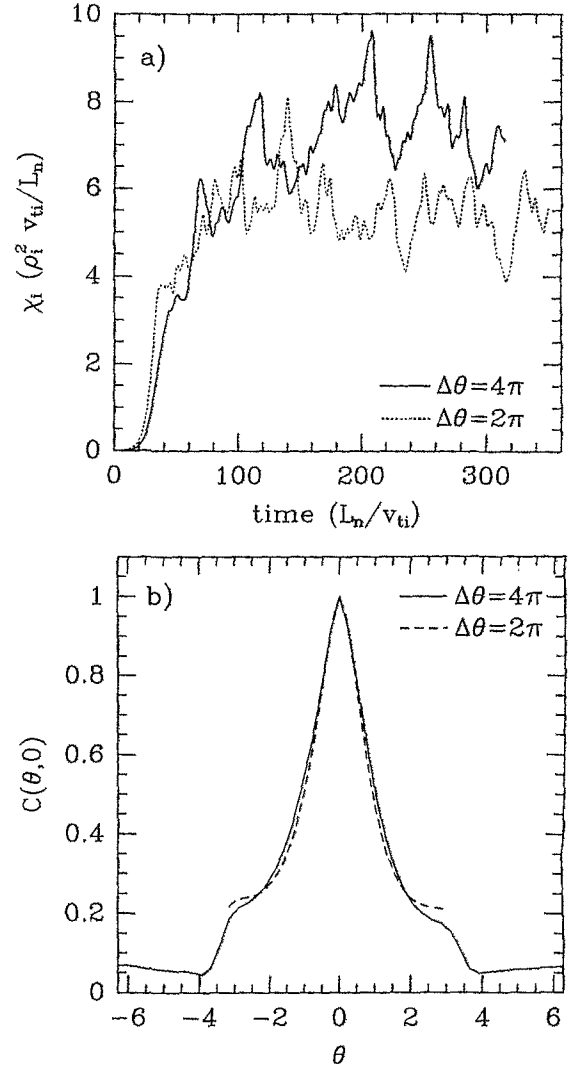


FIG. 7. (a) Evolution of  $\chi_i$  for two runs with varying box length and  $\hat{s}=1.5$ ,  $q=2.4$ . (b) Correlation functions along the field line for the same two runs.

above, except  $\hat{s}=0.1$  and  $q=1.2$ , and the perpendicular box size is  $L_x = 160\rho_i$ ,  $L_y = 100\rho_i$ . Again, the  $\Delta\theta=2\pi$  box gives slightly lower flux, while the longer boxes all give the same flux, so the minimum box length is  $\Delta\theta=4\pi$ . The correlation functions of electron density for these runs are shown in Fig. 8(b), and are noticeably broader than in the higher shear cases. Using  $n_e$  in the correlation functions removes the  $k_{\parallel}=0$  component present in the  $\Phi$  correlation functions in Fig. 7(b), since  $n_e = \Phi - \langle \Phi \rangle$  (see the Appendix). For these low shear runs, the poloidal spectrum peaks at  $k_y \rho_i = 0.35$ , so the perpendicular correlation length is smaller than in the high shear cases. This may contribute to the slightly smaller change in flux in going from  $\Delta\theta=2\pi$  to  $\Delta\theta=4\pi$ , even though the parallel correlation functions are broader. These low shear runs are better resolved than the high shear runs in Fig. 7, so we expect that a 30% change in flux when the artificial correlations are removed by using a longer box is typical for ITG turbulence, where  $\theta_c \sim 2\pi$ . We have also run with  $\hat{s}=0.1$  and  $q=2.4$ , where  $\chi_i = 7.5 \rho_i^2 v_{ti}/L_n$  for  $\Delta\theta=4\pi$  and  $\chi_i = 6.5 \rho_i^2 v_{ti}/L_n$  for  $\Delta\theta$

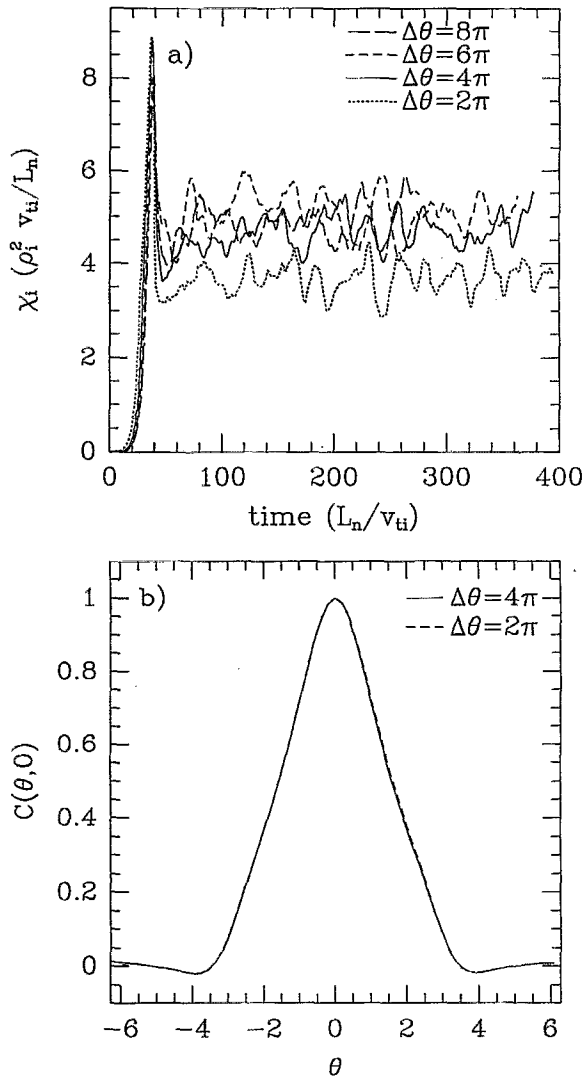


FIG. 8. (a) Evolution of  $\chi_i$  for four runs with varying box length and  $\hat{s}=0.1$ ,  $q=1.2$ . (b) Correlation functions along the field line for  $\Delta\theta=2\pi$  and  $4\pi$ .

$=2\pi$ . For  $\hat{s}=0.25$  and  $q=1.2$ , both  $\Delta\theta=2\pi$  and  $\Delta\theta=4\pi$  give  $\chi_i=5\rho_i^2 v_{ti}/L_n$ , any change is within the statistical fluctuations.

## VII. DISCUSSION AND CONCLUSIONS

To summarize, we are simulating a rectangular domain in  $(x, y, z)$ , and using the transformation Eq. (10), this domain becomes a long, thin, twisting flux tube in a torus. The differential operators take the particularly useful forms Eq. (2)–(6), applicable to general magnetic geometry; only the metric coefficients  $\nabla\alpha$ ,  $\nabla\psi$ , and  $\nabla z$  need to be specified. The boundary condition Eq. (19) can make the perturbations periodic in  $\theta$ , if  $N=1$ , which makes this representation equivalent to the ballooning representation for a coarse grid in  $n$ , with spacing  $n_0$ . However, when  $n_0>1$ , the box must be extended in  $\theta$  to avoid nonphysical correlations if the parallel correlation length is longer than  $2\pi qR$ , i.e.,  $\theta_c>2\pi$ . The fundamental assumptions are that the correlation lengths (both parallel and perpendicular) are smaller than the box size, that the equilibrium gradients vary slowly across the

small perpendicular extent of the box, and that the turbulence is local, i.e., driven only by the equilibrium gradients within the box.

The assumptions implicit in simulating a thin flux-tube subdomain should always be checked *a posteriori* by verifying that the simulation box is indeed at least a few correlation lengths long in each direction, so that the box is large enough for the type of turbulence under consideration. One should also verify that the results are independent of the size of the simulated flux tube (and independent of the particular choice of boundary conditions), as the flux tube is made larger than the correlation lengths. In this paper we have demonstrated that both conditions are met, at least for the particular cases considered in Sec. VI. Our gyrofluid equations have been scaled to the gyroradius  $\rho_i$ , and the limit  $\rho_i/L_n\rightarrow 0$  taken, using the usual small-scale turbulence ordering assumptions, thus the box-size independence implies gyro-Bohm scaling with magnetic field,  $B$ , at least for sufficiently small  $\rho_*=\rho_i/L_n$ .

While the turbulent heat conduction from our simulations is of the right order of magnitude to explain experimental results from the core region of many tokamaks, the experiments indicate a Bohm scaling<sup>27,28</sup> with  $B$ , not gyro-Bohm. Several possibilities for this discrepancy exist. One is that the experimental  $\rho_*$ , while small ( $\sim 10^{-3}$ – $10^{-2}$ ), may be large enough that the radial variation of equilibrium gradients, i.e.,  $\omega_*(\psi)$ ,  $\eta_i(\psi)$ , etc., or equilibrium flows, may be affecting the turbulence. For very small  $\rho_*$  there is a scale separation between the turbulence, with scales of order  $\rho_i$ , and the equilibrium, with scale  $L_n$ , but if  $\rho_*$  is not small enough, the turbulence may begin to feel radial variations in the equilibrium. It is interesting to note that the BES measured<sup>1</sup> correlation length  $\lambda_c\sim 2$  cm is of order of the geometric mean between  $\rho_i\sim 0.15$  cm and the minor radius  $a\sim 90$  cm. Another possible explanation is that the instabilities driving the turbulence may be near marginal stability, which can mask gyro-Bohm scaling trends, and, in some limits, tie the core transport scaling to edge parameters.<sup>29–31</sup> A very sensitive dependence on some parameters that vary slightly while scaling  $\rho_*$  could also partially mask a gyro-Bohm scaling. Another explanation might involve nonlocal turbulence, where fluctuations radially propagate a significant distance from where they were generated by an instability, an effect that is currently under debate.<sup>32,33</sup>

Numerical studies of some of these effects do not necessarily require simulating the whole tokamak. Rather, one could consider a somewhat thicker flux tube than usual, and include the radial variations of  $\omega_*(\psi)$ ,  $\eta_i(\psi)$ , and other plasma parameters over the simulated region. Even if simulating the full torus radially, field-line coordinates are useful to allow a coarser grid in the parallel direction, and a coarser grid in the toroidal mode number  $n$ . When the equilibrium profiles are assumed to be constant, so  $L_n$ ,  $L_T$ , etc., do not vary radially (as assumed in our simulations), the linear eigenmodes are unbounded radially. In ballooning terminology, the solutions of the zeroth-order eigenmode equation in  $1/nq$  are independent of  $\psi$ . In a real tokamak, however, the radial profile variation determines the radial extent of the linear modes, and this radial structure is determined from a

higher-order equation in  $1/nq$ . Recently, there has been renewed interest in the solution for this radial envelope, and the modifications to the zeroth-order eigenfrequencies.<sup>22</sup> For longer-wavelength global modes, the linear radial mode structure is also determined by the radial variation of equilibrium gradients.<sup>34</sup> An alternative way to include these effects is to still use Eq. (7) to represent the perturbations. The  $\psi$  dependence of the equilibrium will then linearly couple different  $j$  modes in Eq. (7), which are uncoupled when the profiles have constant gradients. Then the superposition of different  $j$  (i.e.,  $k_x$ ) modes will determine the radial envelope of the true linear mode. However, since the nonlinear  $\mathbf{E} \times \mathbf{B}$  coupling of the various  $\hat{A}_{j,k}$  modes is usually much stronger than this linear coupling, it is likely that the precise radial linear mode shape is subdominant, and that the radial scale length of the turbulence is set by nonlinear processes, as suggested in Refs. 6 and 35. Comparing the order of magnitude of these effects in, for example, the density equation, we have

$$\frac{1}{n_0} \mathbf{v}_E \cdot \nabla n_1 \sim \rho_i v_{ti} k_\perp^2 \frac{e\Phi}{T_i} \frac{n_1}{n_0},$$

$$\frac{1}{n_0} \mathbf{v}_E \cdot \nabla n_0(x) \sim \frac{\rho_i v_{ti} k_y}{L_n} \frac{e\Phi}{T_i} \left[ 1 + \mathcal{O}\left(\frac{x}{L_*}\right) \right],$$

where  $L_*$  is the scale length for the radial variation in  $L_n$ , and is typically of order  $L_n$ . The nonlinear term is of the same order as the  $x$ -independent linear term [i.e., the  $\omega_*(\psi_0)$  term] in the standard gyrokinetic ordering, where  $n_1/n_0 \sim \rho_i/L_n$  and  $k_\perp \rho_i \approx 1$ . As the linear mode widths get broader radially (in  $x$ ), the  $x/L_*$  terms become more important. While the linear modes are broad, the typical turbulent eddy size is not much larger than  $\Delta x \sim 10\rho_i$ , so it would seem that the  $x$ -dependent term ( $\propto \partial\omega_*/\partial\psi$ ) can safely be ignored, as long as  $\Delta x \ll L_*$ . The effects of radial variations in the equilibrium may start becoming important if  $\rho_* = \rho_i/L_*$  is large enough, and could lead to a transition from gyro-Bohm to Bohm behavior.<sup>36</sup> From the above arguments, it would seem that experiments should have small enough  $\rho_*$  to be in the gyro-Bohm regime, though TFTR seems to be in the Bohm regime.<sup>27,28</sup>

Equilibrium sheared zonal flows ( $k_y=0$ ,  $k_z=0$ ,  $k_x \neq 0$  flows that cause flux surfaces to rotate) can be included in our representation in several ways (one of which is presented in Ref. 19), though we have not yet implemented them in our simulations. Such sheared flows can be important, particularly near the plasma edge, where they appear to be responsible for the H-mode transition.<sup>37</sup> Though we are presently neglecting equilibrium-scale zonal flows, we do include the higher  $k_r$  components of the zonal flows that are generated by the turbulence itself.

For typical tokamak parameters, our reduced simulation volume can represent large computational savings. We compare rough scalings with some other methods; the results are only order of magnitude estimates. Perhaps, the most straightforward way to simulate a tokamak is with the “ $m, n, r$ ” representation:

$$\Phi(\psi, \theta, \zeta) = \sum_{m,n} e^{in\zeta - im\theta} \hat{\Phi}_{m,n}(\psi). \quad (32)$$

Since we are interested in simulating fine-scale turbulence, we need to resolve perpendicular scales of order  $\rho_i$ . If we are simulating a full torus, the range of  $m$ 's must be  $m \in (0, \pm 1, \dots, \pm a/\rho_i)$ . To resolve the long parallel structure, the range of  $n$ 's must be  $n \in (0, \pm 1, \dots, \pm a/q\rho_i)$ , where  $q$  is a representative value, around 2. The radial grid for  $\hat{\Phi}_{m,n}(\psi)$  must resolve  $\rho_i$  and span the minor radius, so  $r = l\Delta_r$ , where  $\Delta_r \sim \rho_i$  and  $l \in (0, 1, \dots, a/\rho_i)$ . This gives the total number of grid points, for  $a \sim 10^3 \rho_i$ ,  $N_{m,n,r} \sim 1/q(a/\rho_i)^3 \sim 10^9$ . This is the same as expected from a computational grid in the physical  $r, \theta, \zeta$  space, where the  $\zeta$  grid can be  $1/q$  coarser than the  $r$  or  $\theta$  directions.

By simulating a thin toroidal annulus in  $r$ , but still going all the way around in  $\theta$  and  $\zeta$ , the number of radial grid points is reduced by  $\Delta_r/a$ , which for our simulations is typically  $\frac{1}{10}$ . Further, aligning the grid points with the field lines reduces the necessary resolution in this direction. We have found that 64 grid points along the field line is adequate, so the number of grid points for a thin annulus with a field-aligned coordinate is  $N_{\text{annulus}} \sim 64(a/\rho_i)^2 \Delta_r/a \sim 10^7$ .

The next level of reduction is to also exploit the small perpendicular correlation length in the poloidal direction, which brings us to our twisting flux tube:  $N_{\text{flux tube}} \sim 64(a/\rho_i)^2 (\Delta_r/a) (\Delta y/a) \sim 10^6$ , so for the simulation in Fig. 5(a), including modes for dealiasing, we used  $N \sim 64 \times 128 \times 48 \times 4 \times 10^5$ . This is roughly  $10^3$  times fewer grid points than a full torus simulation with the same resolution.

Kotschenreuther and Wong<sup>15</sup> have proposed using the representation

$$\Phi(r, \theta, \zeta) = \sum_{j,l} e^{il(m_0\theta - n_0\zeta)} e^{ij\theta} \hat{\Phi}_{j,l}(r - r_0), \quad (33)$$

which has many similarities to our representation. It is periodic in  $\zeta$  with period  $2\pi/n_0$  and in  $\theta$  over  $2\pi$ , and is therefore simulating a wedge of a toroidal annulus when the  $r$  domain is small. Thus, Eq. (33) is as efficient as the one described in this paper, however, if  $\theta_c > 2\pi$ , false correlations along the parallel direction will be introduced, as discussed in Sec. III. It is not obvious how to remedy this problem with Eq. (33), but with our approach one simply uses a longer box, i.e.,  $N > 1$ .

The “quasibalooning” approach of Dimits<sup>16</sup> shares similar computational advantages to our method. Indeed, the quasibalooning (almost-field-line coordinates) method has many similarities to the field-line coordinates approach of Roberts and Taylor,<sup>5</sup> and Cowley *et al.*,<sup>6</sup> upon which our paper is based, though the quasibalooning method emphasizes the perspective of a real-space radial grid, while we use discrete Fourier transforms for the radial direction that illustrate its relation to the usual ballooning transformation. We have shown that physical periodicity in  $\theta$  can also be implemented with our approach, but that there are cases where one should forgo physical periodicity in favor of a longer box (i.e.,  $N > 1$ ) to avoid false parallel correlations. As described

in Sec. III, simulating only  $1/n_0$  of the toroidal direction is often justified by the short perpendicular correlation lengths of the turbulence, but that makes a perturbation extended along a field-line  $n_0$  times as likely to “bite its tail,” which should be compensated for by making the box longer than a parallel correlation length. In principle,  $N=1$  simulations should eventually converge as the box is made large enough in the perpendicular directions (so that  $n_0 \rightarrow 1$ ), but from the runs we have done it appears that faster convergence is obtained by allowing the box to be longer than a parallel correlation length as well, thus consistently following the principle that the simulation domain should be longer than the correlation lengths in all three directions.

## ACKNOWLEDGMENTS

The authors thank R. E. Waltz and G. D. Kerbel for useful discussions. Our toroidal nonlinear gyrofluid code grew out of the earlier slab gyrofluid code developed by W. Dorland,<sup>10,38</sup> who provided helpful computational advice and physics discussions. M.A.B. also thanks Q. P. Liu, D. P. Coster, and M. Artun for further useful discussions and computational advice.

M.A.B. and G.W.H. thank the TFTR project for supporting this work, and the National Energy Research Supercomputer Center for computing resources. This work was supported in part by the High Performance Computing and Communications Initiative (HPCCI) Grand Challenge Numerical Tokamak Project, by U.S. Department of Energy Contract No. DE-AC02-76-CH0-3073, Contract No. DE-FG03-93ER54224, and by a National Science Foundation Graduate Fellowship.

## APPENDIX: TOROIDAL GYROFLUID EQUATIONS

The equations used in the simulations are a subset of those derived in detail in Ref. 8, and are briefly summarized here. In these simulations, we evolve four moments of the gyrokinetic equation, the perturbed guiding center density, parallel flow, parallel temperature, and perpendicular temperature, with closure approximations to model the effects of parallel resonances,<sup>25</sup> toroidal resonances,<sup>39,40</sup> and FLR.<sup>41</sup> Here we ignore collisions and particle trapping (i.e.,  $\hat{\mathbf{b}} \cdot \nabla B = 0$ ), although we have developed models of these effects, and have extended this model to up to six moments.<sup>7</sup> Using the normalizations in Ref. 41, the dynamical equations are

$$\begin{aligned} \frac{dn}{dt} + \hat{\mathbf{b}} \cdot \nabla u_{\parallel} + \left(1 + \frac{\eta_i}{2} \hat{\nabla}_{\perp}^2\right) \frac{\partial \Psi}{\partial y} + \left(\frac{1}{2} \hat{\nabla}_{\perp}^2 \mathbf{v}_{\Psi}\right) \cdot \nabla T_{\perp} &= -i\omega_d(T_{\parallel} + T_{\perp} + 2n + 2\Psi), \\ \frac{du_{\parallel}}{dt} + \hat{\mathbf{b}} \cdot \nabla (T_{\parallel} + n + \Psi) &= -2i\omega_d \nu_{Si} u_{\parallel} - 2|\omega_d| \nu_{Sr} u_{\parallel}, \\ \frac{dT_{\parallel}}{dt} + 2\hat{\mathbf{b}} \cdot \nabla u_{\parallel} + \sqrt{2}|k_{\parallel}| \chi_{\parallel} T_{\parallel} + \eta_i \frac{\partial \Psi}{\partial y} &= -2i\omega_d[(3 + \nu_{1i})T_{\parallel} + \nu_{2i}T_{\perp} + n + \Psi] - 2\nu_{1r}|\omega_d|T_{\parallel} - 2\nu_{2r}|\omega_d|T_{\perp}, \\ \frac{dT_{\perp}}{dt} + \sqrt{2}|k_{\parallel}| \chi_{\perp} \left(T_{\perp} + \frac{1}{2} \hat{\nabla}_{\perp}^2 \Psi\right) + \left(\frac{1}{2} \hat{\nabla}_{\perp}^2 + \eta_i(1 + \hat{\nabla}_{\perp}^2)\right) \frac{\partial \Psi}{\partial y} &+ \left(\frac{1}{2} \hat{\nabla}_{\perp}^2 \mathbf{v}_{\Psi}\right) \cdot \nabla n + (\hat{\nabla}_{\perp}^2 \mathbf{v}_{\Psi}) \cdot \nabla T_{\perp} \\ &= -2i\omega_d \left[\nu_{3i}T_{\parallel} + (2 + \nu_{4i})T_{\perp} + \frac{n}{2} + \frac{1}{2} \left(1 + \frac{3}{2} \hat{\nabla}_{\perp}^2\right) \Psi\right] - 2\nu_{3r}|\omega_d|T_{\parallel} - 2\nu_{4r}|\omega_d|T_{\perp}. \end{aligned}$$

The total time derivative includes the  $\mathbf{E} \times \mathbf{B}$  nonlinearities,  $d/dt = \partial/\partial t + \mathbf{v}_{\Psi} \cdot \nabla$ . The gyroaveraged potential and  $\mathbf{E} \times \mathbf{B}$  drift are  $\Psi = \Gamma_0^{1/2} \Phi$  and  $\mathbf{v}_{\Psi} = \hat{\mathbf{b}} \times \nabla \Psi$ , respectively. The toroidal drift terms have been written using  $i\omega_d \equiv (cT/eB^2) \mathbf{B} \times \nabla B \cdot \nabla$ .

The closure coefficients for this set of moments are chosen to provide an accurate approximation to the linear kinetic response. The parallel closure coefficients are  $\chi_{\parallel} = 2/\sqrt{\pi}$  and  $\chi_{\perp} = 1/\sqrt{\pi}$ . The toroidal closure coefficients have both dissipative and reactive pieces, and written in the form  $\nu = (\nu_r, \nu_i) = \nu_r + i\nu_i|\omega_d|/\omega_d$ , they are  $\nu_1 = (1.93, -0.39)$ ,  $\nu_2 = (0.24, 1.29)$ ,  $\nu_3 = (-1.40, 0.47)$ ,  $\nu_4 = (-0.14, -1.75)$ , and  $\nu_5 = (0.76, -0.98)$ .

We assume the adiabatic electron response,  $n_e = \tau(\Phi - \langle \Phi \rangle)$ , where  $\tau = T_i/T_e$ , and  $\langle \Phi \rangle(\psi) = (\int d\alpha dz J|\nabla \psi| \Phi) / (\int d\alpha dz J|\nabla \psi|)$  is a flux surface average. In circular concentric geometry, this becomes

$\langle \Phi \rangle = (4 \Delta y z_0)^{-1} \int dy dz (R/R_0) \Phi(x, y, z)$ , and is only nonzero for the  $k_y = 0$  components. This form of the adiabatic electron response prevents radial electron flow, which would short out the radial electric field responsible for the nonlinearly generated sheared  $\mathbf{E} \times \mathbf{B}$  flows that are essential for saturation.<sup>7</sup> The gyrokinetic quasineutrality constraint is  $n_e = \bar{n}_i + (\Gamma_0 - 1)\Phi$ , where  $\bar{n}_i$  is the ion density in real space, which is related to the ion guiding center density and perpendicular temperature by the FLR closure relation in Ref. 41, yielding

$$\tau(\Phi - \langle \Phi \rangle) = \frac{\Gamma_0^{1/2}}{D(b)} \left( N(b)n + \frac{1}{2} \hat{\nabla}_{\perp}^2 T_{\perp} \right) + (\Gamma_0 - 1)\Phi.$$

The functions  $N(b)$  and  $D(b)$ , where  $b = k_{\perp}^2 \rho_i^2$ , and the operators  $\hat{\nabla}_{\perp}$  and  $\hat{\nabla}_{\perp}^2$  model FLR effects, and explicit forms are given in Ref. 41. Since this equation involves both  $\Phi$  and  $\langle \Phi \rangle$ , we use the following procedure to determine  $\Phi$ , given  $n$

and  $T_{\perp}$ . In general, the coefficients in this equation can be functions of the field-line coordinate, so writing  $\Phi = \langle \Phi \rangle + \delta\Phi$ , and solving for  $\delta\Phi$  gives  $\delta\Phi = [\bar{n}_i + (\Gamma_0 - 1)\langle \Phi \rangle]/(\tau + 1 - \Gamma_0)$ . Now flux surface averaging  $\delta\Phi$ , since  $\langle \delta\Phi \rangle = 0$ , and solving for  $\langle \Phi \rangle$ , gives

$$\langle \Phi \rangle = \left\langle \frac{\bar{n}_i}{\tau + 1 - \Gamma_0} \right\rangle \left/ \left\langle \frac{(1 - \Gamma_0)}{\tau + 1 - \Gamma_0} \right\rangle \right.$$

Now that  $\langle \Phi \rangle$  is determined, we use this expression in the quasineutrality constraint to obtain  $\Phi$ .

- <sup>1</sup>R. J. Fonck, G. Cosby, R. D. Durst, S. F. Paul, N. Bretz, S. Scott, E. Synakowski, and G. Taylor, *Phys. Rev. Lett.* **70**, 3736 (1993).
- <sup>2</sup>E. Mazzucato and R. Nazikian, *Phys. Rev. Lett.* **71**, 1840 (1993).
- <sup>3</sup>S. Zweben and S. S. Medley, *Phys. Fluids B* **1**, 2058 (1989).
- <sup>4</sup>S. E. Parker, J. C. Cummings, W. W. Lee, and H. E. Mynick, in *Proceedings of the Joint Varenna-Lausanne International Workshop on Theory of Fusion Plasmas* (Societa Italiana di Fisica, Bologna, 1994).
- <sup>5</sup>K. V. Roberts and J. B. Taylor, *Phys. Fluids* **8**, 315 (1965).
- <sup>6</sup>S. C. Cowley, R. M. Kulsrud, and R. Sudan, *Phys. Fluids B* **3**, 2767 (1991).
- <sup>7</sup>G. W. Hammett, M. A. Beer, W. Dorland, S. C. Cowley, and S. A. Smith, *Plasma Phys. Controlled Fusion* **35**, 973 (1993).
- <sup>8</sup>M. A. Beer, Ph.D. thesis, Princeton University, 1994.
- <sup>9</sup>M. D. Kruskal and R. M. Kulsrud, *Phys. Fluids* **1**, 265 (1958).
- <sup>10</sup>W. Dorland, G. W. Hammett, T. S. Hahm, and M. A. Beer, in *U.S.-Japan Workshop on Ion Temperature Gradient Driven Turbulent Transport*, edited by W. Horton, M. Wakatani, and A. Wootton (American Institute of Physics, New York, 1993), p. 344.
- <sup>11</sup>B. Cohen, T. J. Williams, A. M. Dimits, and J. A. Byers, *Phys. Fluids B* **5**, 2967 (1993).
- <sup>12</sup>A. Hasegawa and M. Wakatani, *Phys. Rev. Lett.* **59**, 1581 (1987).
- <sup>13</sup>B. A. Carreras, V. E. Lynch, and L. Garcia, *Phys. Fluids B* **3**, 1438 (1991).
- <sup>14</sup>P. H. Diamond and Y. B. Kim, *Phys. Fluids B* **3**, 1626 (1991).
- <sup>15</sup>M. Kotschenreuther and H. V. Wong (private communication, 1991).
- <sup>16</sup>A. M. Dimits, *Phys. Rev. E* **48**, 4070 (1993).
- <sup>17</sup>J. M. Greene and J. L. Johnson, *Phys. Fluids* **5**, 510 (1962).
- <sup>18</sup>R. E. Waltz and A. H. Boozer, *Phys. Fluids B* **5**, 2201 (1993).
- <sup>19</sup>R. E. Waltz, G. D. Kerbel, and J. Milovich, *Phys. Plasmas* **1**, 2229 (1994).
- <sup>20</sup>M. C. Zarnstorff, S. Batha, A. Janos, F. L. Levinton, and the TFTR Group, in *Local Transport Studies in Fusion Plasmas*, edited by J. D. Callen, G. Gorini, and E. Sindoni (Societa Italiana di Fisica, Bologna, 1993), p. 257.
- <sup>21</sup>J. W. Connor, R. J. Hastie, and J. B. Taylor, *Proc. R. Soc. London Ser. A* **365**, 1 (1979); A. H. Glasser, in *Proceedings of the Finite Beta Theory Workshop*, Varenna, 1977, edited by B. Coppi and W. Sadowski (U.S. Department of Energy, Washington, DC, 1977), CONF-7709167, p. 55; Y. C. Lee and J. W. Van Dam, *ibid.* p. 93.
- <sup>22</sup>J. W. Connor, J. B. Taylor, and H. R. Wilson, *Phys. Rev. Lett.* **70**, 1803 (1993); J. B. Taylor, J. W. Connor, and H. R. Wilson, *Plasma Phys. Controlled Fusion* **35**, 1063 (1993); N. Mattor, *Phys. Plasmas* **1**, 245 (1994).
- <sup>23</sup>R. D. Hazeltine and W. A. Newcomb, *Phys. Fluids B* **2**, 7 (1990).
- <sup>24</sup>E. A. Frieman and L. Chen, *Phys. Fluids* **25**, 502 (1982).
- <sup>25</sup>G. W. Hammett and F. W. Perkins, *Phys. Rev. Lett.* **64**, 3019 (1990).
- <sup>26</sup>R. J. Hawryluk, D. Mueller, J. Hosea, C. W. Barnes, M. A. Beer, M. G. Bell, R. Bell, H. Biglari, M. Bitter, R. Boivin, N. L. Bretz, R. V. Budny, C. E. Bush, L. Chen, C. Cheng, S. Cowley, D. Darrow, P. C. Efthimion, R. J. Fonck, E. Frederickson, H. P. Furth, G. Greene, B. Grek, L. R. Grisham, G. W. Hammett, W. W. Heidbrink, K. W. Hill, D. Hoffman, R. Hulse, H. Hsuan, A. Janos, D. L. Jassby, F. C. Jobes, D. W. Johnson, L. C. Johnson, R. Kamperschroer, J. Kesner, C. Phillips, S. J. Kilpatrick, H. Kugel, P. H. LaMarche, B. LeBlanc, D. M. Manos, D. K. Mansfield, E. Marmar, E. Mazzucato, M. P. McCarthy, J. Machuzak, M. Mauel, D. C. McCune, K. McGuire, S. S. Medley, D. R. Mikkelsen, D. Monticello, Y. Nagayama, G. Navratil, R. Nazikian, D. K. Owens, H. Park, W. Park, S. F. Paul, F. W. Perkins, S. Pitcher, D. Rasmussen, M. H. Redi, G. Rewoldt, D. Roberts, A. L. Roquemore, S. Sabbagh, G. Schilling, J. Schivell, G. L. Schmidt, S. D. Scott, J. Snipes, J. Stevens, W. Stodiek, B. C. Stratton, J. Strachan, E. Synakowski, W. M. Tang, G. Taylor, J. Terry, J. R. Timberlake, H. H. Towner, M. Ulrickson, S. von Goeler, R. Wieland, J. Wilson, K. L. Wong, P. Woskov, M. Yamada, K. M. Young, M. C. Zarnstorff, and S. J. Zweben, *Fusion Technol.* **21**, 1324 (1992).
- <sup>27</sup>S. D. Scott, C. W. Barnes, D. M. Mikkelsen, F. W. Perkins, M. G. Bell, R. E. Bell, C. E. Bush, D. E. Ernst, E. D. Fredrickson, B. Grek, K. W. Hill, A. C. Janos, F. C. Jobes, D. W. Johnson, D. K. Mansfield, D. K. Owens, H. Park, S. F. Paul, A. T. Ramsey, J. Schivell, B. C. Stratton, E. J. Synakowski, W. M. Tang, and M. C. Zarnstorff, in *Plasma Physics and Controlled Nuclear Fusion Research 1992* (International Atomic Energy Agency, Vienna, 1993), Vol. 3, p. 427.
- <sup>28</sup>F. W. Perkins, C. W. Barnes, D. W. Johnson, S. D. Scott, M. C. Zarnstorff, M. G. Bell, R. E. Bell, C. E. Bush, B. Grek, K. W. Hill, D. K. Mansfield, H. Park, A. T. Ramsey, J. Schivell, B. C. Stratton, and E. Synakowski, *Phys. Fluids B* **5**, 477 (1993).
- <sup>29</sup>P. W. Terry, J.-N. Leboeuf, P. H. Diamond, D. R. Thayer, J. E. Sedlak, and G. S. Lee, *Phys. Fluids* **31**, 2920 (1988).
- <sup>30</sup>H. Biglari, P. H. Diamond, and M. N. Rosenbluth, *Phys. Fluids B* **1**, 109 (1989).
- <sup>31</sup>M. Kotschenreuther, H. L. Berk, M. Lebrun, J. Q. Dong, W. Horton, J.-Y. Kim, Y. Kishimoto, D. W. Ross, T. Tajima, P. M. Valanju, H. V. Wong, W. Miner, D. C. Barnes, J. U. Brackbill, K. M. Ling, R. A. Nebel, W. D. Nystrom, J. A. Byers, B. I. Cohen, A. M. Dimits, L. L. Lodestro, N. Mattor, G. R. Smith, T. J. Williams, G. D. Kerbel, J. M. Dawson, R. D. Sydora, B. A. Carreras, N. Dominguez, C. L. Hedrick, J.-N. Leboeuf, H. Naitou, and T. Kamimura, in Ref. 27, Vol. 2, p. 11.
- <sup>32</sup>X. Garbet, L. Laurent, J. P. Roubin, and A. Samain, in Ref. 27, Vol. 2, p. 213.
- <sup>33</sup>N. Mattor and P. H. Diamond, *Phys. Rev. Lett.* **72**, 486 (1994).
- <sup>34</sup>W. M. Tang and G. Rewoldt, *Phys. Fluids B* **5**, 2451 (1993).
- <sup>35</sup>N. Mattor, *Phys. Fluids B* **3**, 1913 (1991).
- <sup>36</sup>G. W. Hammett, M. A. Beer, J. C. Cummings, W. Dorland, W. W. Lee, H. E. Mynick, S. E. Parker, R. A. Santoro, M. Artun, H. P. Furth, T. S. Hahm, G. Rewoldt, W. M. Tang, R. E. Waltz, G. D. Kerbel, and J. Milovich, "Advances in simulating tokamak turbulent transport," in *Plasma Physics and Controlled Nuclear Fusion Research 1994*, Paper No. IAEA-CN-60/D-2-II-1 (International Atomic Energy Agency, Vienna, in press).
- <sup>37</sup>H. Biglari, P. H. Diamond, and P. W. Terry, *Phys. Fluids B* **2**, 1 (1990).
- <sup>38</sup>W. Dorland, Ph.D. thesis, Princeton University, 1993.
- <sup>39</sup>R. E. Waltz, R. R. Dominguez, and G. W. Hammett, *Phys. Fluids B* **4**, 3138 (1992).
- <sup>40</sup>M. A. Beer, G. W. Hammett, W. Dorland, and S. C. Cowley, *Bull. Am. Phys. Soc.* **37**, 1478 (1992).
- <sup>41</sup>W. Dorland and G. W. Hammett, *Phys. Fluids B* **5**, 812 (1993).